



Aircraft wing skin contouring as a result of residual stress distributions induced by shot peening  
by Scot Edward Homer

A thesis submitted in partial fulfillment of the requirements for the degree of Master of Science in  
Engineering Mechanics

Montana State University

© Copyright by Scot Edward Homer (1989)

Abstract:

Shot peening is a viable method for the forming of aircraft wing skins to aerodynamic contours. Presently, geometric methods used to calculate peening intensity patterns are approximate. These methods are based on simplifying assumptions which are not valid for complex contours. The scope of the work presented in this thesis is to develop a more accurate method of predicting peening intensity patterns.

The finite element is used to model the effects of shot peening. Inversion of the equations to determine an exact solution for the peening intensity pattern is impossible. An approximate solution is found through numerical methods taking into account contour accuracy and peening intensity magnitudes.

The resulting procedure produces accurate and reasonable results for the test cases presented, (computer simulations). Verification of the procedure will be completed when the system is field tested on an actual wing skin.

AIRCRAFT WING SKIN CONTOURING AS A RESULT OF RESIDUAL  
STRESS DISTRIBUTIONS INDUCED BY SHOT PEENING

by

Scot Edward Homer

A thesis submitted in partial fulfillment  
of the requirements for the degree

of

Master of Science

in

Engineering Mechanics

MONTANA STATE UNIVERSITY  
Bozeman, Montana

August 1989

N378  
H7525

APPROVAL

of a thesis submitted by

Scot Edward Homer

This thesis has been read by each member of the thesis committee and has been found to be satisfactory regarding content, English usage, format, citations, bibliographic style, and consistency, and is ready for submission to the College of Graduate Studies.

8/9/89  
Date

R. Daniel Co. Luchman  
Chairperson, Graduate Committee

Approved for the Major Department

10 Aug '89  
Date

Therese E. Long  
Head, Major Department

Approved for the College of Graduate Studies

August 18, 1989  
Date

Henry T. Parsons  
Graduate Dean

## STATEMENT OF PERMISSION TO USE

In presenting this thesis in partial fulfillment of the requirements for a master's degree at Montana State University, I agree that the Library shall make it available to borrowers under rules of the Library. Brief quotations from this thesis are allowable without special permission, provided that accurate acknowledgment of source is made.

Permission for extensive quotation from or reproduction of this thesis may be granted by my major professor, or in his absence, by the Dean of Libraries when, in the opinion of either, the proposed use of the material is for scholarly purposes. Any copying or use of the material in this thesis for financial gain shall not be allowed without my written permission.

Signature Scott Homer

Date 8-17-89

## ACKNOWLEDGEMENTS

The author would like to express sincere thanks to Dr. R.D. VanLuchene for the guidance and insight he provided during the course of this investigation.

The author also gratefully acknowledges The Boeing Airplane Company for their support of this work. The project has been a rewarding endeavor.

## TABLE OF CONTENTS

	Page
LIST OF FIGURES .....	vii
ABSTRACT .....	x
I. INTRODUCTION .....	1
Mechanics of a Single Shot Impact .....	2
Macroscopic Effects .....	4
Application to Commercial Aircraft Wing Skins .....	8
II. STRESS DISTRIBUTION ON THE CROSS SECTION .....	13
Effects of Nonlinear Material Behavior .....	14
Net Effect of the Initial Stress Distribution .....	18
Mathematical Forms for the Initial Stress Distribution .....	19
Spherical Cavity Model .....	19
Thick Section Empirical Model .....	22
Conclusions .....	26
III. DEFLECTION CALCULATIONS .....	28
Elastic Response in Terms of Peening Intensity .....	29
Second Order Effects .....	31
Finite Element Modeling of Shot Peening .....	33
Effects of the Assembly Process .....	34
Nonlinear Considerations .....	36
Software .....	37

IV.	PEENING INTENSITY PATTERN CALCULATIONS .....	38
	Geometric Method .....	38
	Theoretical Problems with the Geometric Method .....	39
	Calculation of $\epsilon$ .....	40
	Definition of the Neutral Axis .....	41
	Coupling Between Chordwise and Spanwise Peening ..	44
	Application of Empirical Equations .....	45
	Practical Considerations .....	46
	Finite Element Based Method .....	46
	Displacements Due to Stress Intensities .....	47
	Approximate Solution .....	49
	Constraints on the Stress Intensities .....	50
	Decomposition of the Error Function .....	50
	Calculation of [P] .....	54
V.	RESULTS .....	56
	Example Problems .....	56
	Example 1 - Twisted Contour .....	58
	Example 2 - Spherical Contour .....	62
	Example 3 - Gull Wing Contour .....	65
	Variation of the Penalty Scale Factor .....	71
	Application .....	74
	Error Induced by Negative Required Growth .....	81
VI.	SUMMARY .....	84
	REFERENCES .....	89

## LIST OF FIGURES

Figure		Page
1	Plastically Deformed Zone. ....	3
2	Material Flow Due to Impact. ....	4
3	Residual Stress Distribution in a Uniformly Peened Plate. ....	5
4	Curvature Development and Growth Due to Shot Peening. ....	7
5	Fanning and Overall Growth. ....	9
6	Typical Residual Stress in a Thin Plate. ....	13
7	Piecewise Linear Modulus of Elasticity. ....	15
8	Normalized In-plane Stress for Piecewise Linear Modulus of Elasticity. ....	17
9	Normalized Bending Stress for Piecewise Linear Modulus of Elasticity. ....	17
10	Initial Stress Based on Spherical Cavity Model. ....	20
11	Normalized In-plane Stress Resultant. ....	21
12	Normalized Bending Stress Resultant. ....	22
13	Initial Stress Based on Thick Section Empirical Model. ....	23
14	Normalized In-plane Stress Resultant. ....	24
15	Normalized Bending Stress Resultant. ....	24
16	Residual Stress Based on Thick Section Empirical Model. ....	25
17	Nodal Equivalent Loads Due to Shot Peening. ....	34
18	General Saddle Contour Geometry. ....	39

## LIST OF FIGURES - CONTINUED

Figure	Page
19	Calculation of Required Growth - Geometric Method. . . . . 40
20	Actual Spanwise Radius of Curvature at a Point Away from the Neutral Axis. . . . . 41
21	Twisted Contour. . . . . 43
22	Rotated Coordinate System. . . . . 43
23	Boundary between Regions of Different Peening Intensity. . . . . 45
24	Iterative Procedure for Calculating Peening Intensities. . . . . 55
25	Finite Element Mesh. . . . . 57
26	Twisted Contour, (not to scale). . . . . 59
27	Required Growth for Twisted Contour, (not to scale). . . . . 60
28	Required Curvature for Twisted Contour, (not to scale). . . . . 61
29	Contour Error - Twisted Contour, (not to scale). . . . . 62
30	Spherical Contour, (not to scale). . . . . 63
31	Required Growth for Spherical Contour, (not to scale). . . . . 64
32	Required Curvature for Spherical Contour, (not to scale). . . . . 64
33	Contour Error - Spherical Contour, (not to scale). . . . . 65
34	Gull Wing Contour, (not to scale). . . . . 66
35	Required Growth for Gull Wing Contour, (not to scale). . . . . 67

## LIST OF FIGURES - CONTINUED

Figure	Page
36	Required Curvature for Gull Wing Contour, (not to scale). . . . . 68
37	Contour Error - Gull Wing Contour, (not to scale). . . . . 69
38	Gull Wing Contour - Deflection Due to In-plane Stress, (not to scale). . . . . 70
39	Gull Wing Contour - Deflection Due to Bending Stress, (not to scale). . . . . 70
40	Deviation Norm and Maximum Deviation for Gull Wing Contour. . . . . 72
41	Required Iterations for Gull Wing Contour. . . . . 72
42	Required Curvature for Gull Wing Contour, $k_p = 0.00001$ . . . . . 73
43	Finite Element Mesh - 767 Upper Panel No. 2. . . . . 75
44	Thickness Variation. . . . . 75
45	767 Upper Panel No. 2 Contour, (not to scale). . . . . 76
46	Required Growth Calculated by the Finite Element Based Method. . . . . 78
47	Required Growth Calculated by the Geometric Method. . . . . 78
48	Required Curvature Calculated by the Finite Element Based Method. . . . . 80
49	Required Curvature Calculated by the Geometric Method. . . . . 80

## ABSTRACT

Shot peening is a viable method for the forming of aircraft wing skins to aerodynamic contours. Presently, geometric methods used to calculate peening intensity patterns are approximate. These methods are based on simplifying assumptions which are not valid for complex contours. The scope of the work presented in this thesis is to develop a more accurate method of predicting peening intensity patterns.

The finite element is used to model the effects of shot peening. Inversion of the equations to determine an exact solution for the peening intensity pattern is impossible. An approximate solution is found through numerical methods taking into account contour accuracy and peening intensity magnitudes.

The resulting procedure produces accurate and reasonable results for the test cases presented, (computer simulations). Verification of the procedure will be completed when the system is field tested on an actual wing skin.

## CHAPTER I

### INTRODUCTION

Shot peening is a process whereby the surface of a metal part is treated by repeatedly impacting it with small particles or shot. The treated part has improved resistance to fatigue and to stress corrosion cracking as well as a hardened surface. These beneficial effects of shot peening are well documented and the process has been widely used for many years to extend the useful life and reliability of metal parts. [1-3]

More recently shot peening has become increasingly important as a metal forming process. The process, known as peen forming, has the same beneficial effects mentioned above. In addition, if applied to a part of relatively low stiffness such as a thin plate, peen forming has the effect of changing the shape of the part. The metal forming aspect of the shot peening process, specifically applied to aircraft wing skins, is the topic of this investigation.

In practice, shot peening is accomplished by forcing a stream of spherical particles, usually glass, cast iron, or steel, to strike the surface of a part at high velocity. The shot particles can be propelled through a nozzle by compressed air or thrown radially from the hub of a rotating hollow wheel with radial partitions. In some applications the shot particles are simply allowed to fall onto the part under the influence of gravity. Depending on the equipment, the shot velocity is controlled by varying the air pressure, wheel speed, or the height from which the shot particles fall. In wheel-type machines the shot velocity

is almost entirely dependent on wheel speed. This allows for more precise process control than with air-type machines. Also, relatively high shot velocities can be achieved without the necessity of dropping the shot particles from excessive heights. Typical shot velocities range from 100 to 250 ft/sec (30.5 to 76.2 m/sec). Shot sizes typically range from 0.023 inches (0.058 cm) to 0.125 inches (0.318 cm) in diameter. [4]

### Mechanics of a Single Shot Impact

Each shot particle leaves a small spherical indentation after impact indicating that the surface of the material has undergone local plastic deformation. The plastic deformation of the material in the immediate vicinity of the impact is the mechanism by which shot peening is effective. Thus shot peening is usually only applied to ductile materials.

After a ductile material has been plastically deformed and all external loads are removed, it does not return to its original shape. The material is said to have a permanent "set" or plastic strain. Plastic deformation due to a single shot particle impact is a local effect and therefore the plastic strain is also local. Deformations are required to be continuous at the boundary between the plastically deformed zone and the surrounding elastic material. This causes strains in the elastic material. The elastic and plastic strains in the plastically deformed zone and the purely elastic strains in the surrounding elastic zone generate stresses that remain present after the shot particle has rebounded from the surface. Stresses that are present in a material that is not under the influence of any external loadings, including those produced by inertial and thermal effects, are called residual stresses. [11]

The plastically deformed zone extends radially in all directions around the indentation and into the material to a depth,  $h_p$ , as shown in Figure 1. The shape of the plastically deformed zone is given in references [6,7] and is based on a Hertz analysis of an elastic half-space using the Tresca maximum shear stress criteria for plastic yielding. [11,14] Al-Hassani, [6], states that experiments have shown a similar shape to that of the Hertz analysis.

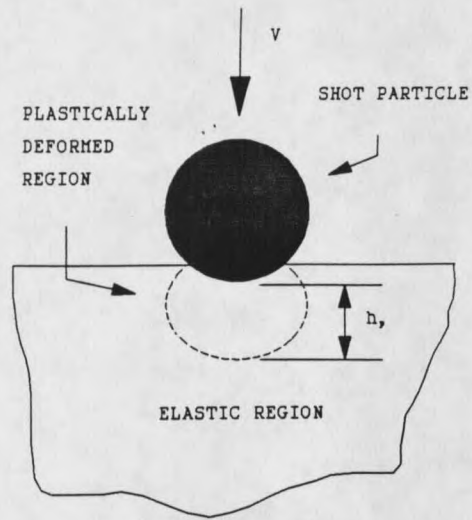


Figure 1. Plastically Deformed Zone.

The depth of the plastically deformed zone depends on the size, density, hardness, speed, and angle of incidence of the shot particle, and on the properties of the material being peened. When dynamical aspects are considered,  $h_p$  is given by

$$h_p = 2.322R(\rho V^2/3Y)^{1/4} \quad (1)$$

where  $\rho$  is the shot density,  $V$  is the shot velocity,  $R$  is the shot radius, and  $Y$  is the material yield stress. [6] Typically, the value of  $h_p$  is much less than both the diameter of the shot particle and the part thickness. Assuming an angle of incidence of 90 degrees and the following values for  $R$ ,  $\rho$ ,  $V$ , and  $Y$ , equation (1) yields a value of  $h_p$  equal to 0.047 inches (0.119 cm).

$$R = 0.0625 \text{ in (0.1588 cm)}$$

$$\rho = 487 \text{ lb/ft}^3 \text{ (76.5 kN/m}^3\text{) (steel)}$$

$$V = 137.5 \text{ ft/sec (41.9 m/sec)}$$

$$Y = 60 \text{ ksi (0.414 GPa) (aluminum)}$$

References [1,2] present a general overview of the effect of these variables and process limitations. References [6,7] present a detailed analysis of the development of the plastic zone due to a single shot impact.

When a shot particle impacts the surface of the part, the material is compressed in the direction normal to the surface and stretched in the direction tangent to the surface. The tangential stretching places surface material in tension. As the elastic limits are exceeded, the material is forced to flow plastically in the direction tangent to the surface as shown in Figure 2. The plastic flow of the surface material is resisted by the

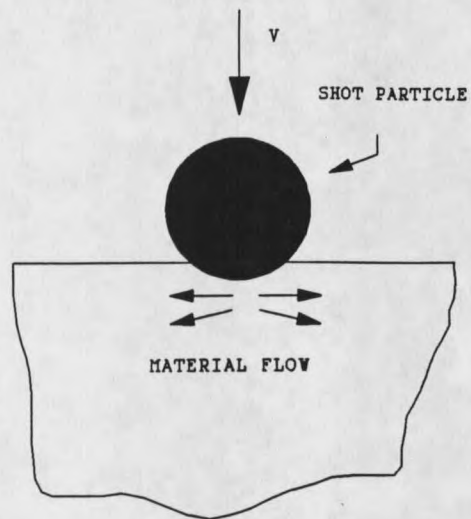


Figure 2. Material Flow Due to Impact.

underlying elastic material. Upon rebound of the shot particle, the stress in the plastically deformed zone reverses, leaving it in a state of residual compression. Static equilibrium is maintained as the surrounding elastic material is left in a state of residual tension. [1,2,6,7]

### Macroscopic Effects

When the part has been peened uniformly over the entire surface, the result is a uniform layer of surface material that has been plastically deformed. The layer of surface material is in a state of residual compression while the underlying elastic material is in a state of residual tension. [1,6,7] The residual stress distribution becomes a function of the

depth only. Furthermore, the stress is invariant under rotations in the plane tangent to the surface.

At this point another process variable, that of percent coverage, may be introduced. Shot peening may be applied to a part in a uniform manner with unaffected areas between individual shot impacts. Percent coverage is defined as the percentage of total surface area that has been indented by individual shot particles. Percent coverage of a surface can be controlled by varying the time of exposure to the shot stream. The effects of percent coverage and methods of measurement are discussed in references [1,2,7,8].

Percent coverage and shot velocity are the two most easily controlled process variables. This allows for the precise control of peening intensity necessary to achieve a desired contour.

The stress due to shot peening has the effect of producing a net bending moment and net normal force on the cross section. Relatively stiff parts, (thick sections), will not show an appreciable deformation due to these forces. Parts of relatively low stiffness, (thin sections), however, will deform significantly. [6,7] Figure 3 shows a residual stress distribution typical of a plate that has been peened uniformly on both sides with the same intensity. [2]

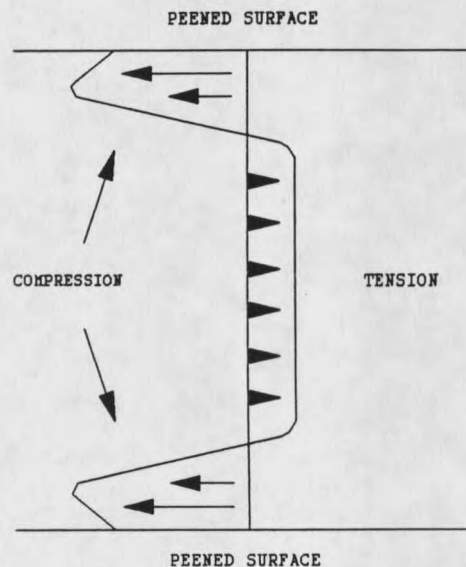


Figure 3. Residual Stress Distribution in a Uniformly Peened Plate.

The residual stress distribution of Figure 3 is based on several simplifying assumptions. The actual stress will vary in the plane tangent to the surface near individual shot particle impacts, especially if the coverage is less than 100%. Invariance of the stress under rotations in the plane tangent to the surface is due to the radial symmetry of the shot particles and an assumed 90 degree angle of incidence of the shot stream. Angles of incidence of individual shot particles will not, in general, be 90 degrees however. Collisions with shot particles rebounding from the surface will cause the angle of incidence to vary for individual shot particles. The fact that the normal stress on a free edge is zero implies that the residual stress distribution of Figure 3 is not valid near sharp edges or corners. This investigation is primarily concerned with the very thin plates used in the manufacture of commercial aircraft wing skins. Edge effects, as well as stresses in the direction normal to the plate, are therefore assumed to have a negligible effect on the overall deformation of the plate.

The assumptions of the preceding paragraph are accepted in this work allowing the residual stress at a specific point on the plate to be described by a scalar function of the depth. Other standard assumptions made in thin plate and shell theory such as "Straight lines normal to the neutral surface remain straight." are accepted as valid on a macroscopic scale as well. [12,13]

The author of references [6,7] questions the validity of these assumptions. Quoting Al-Hassani, [7] pp. 10:

There has been a tendency in the shot peening literature to interpret the residual stress in the component as if it were the result of a stretching action, uniformly and instantaneously distributed over the surface followed by an elastic unloading action again distributed uniformly over the entire length of the specimen. Consequently, simple beam and plate bending theories are then used to explain the general features of the process. In addition to the neglect of the history of the residual stresses, such a concept

relies on a major assumption that plane sections in the plate remain plane. Due to the very local nature of the plastic deformation, the last assumption seriously departs from physical reality. However, such concepts are quite efficient when used in interpreting arc height variation due to the removal of top surface layers.

In this work local variations in the stress field, angle of incidence, and distortion of lines normal to the neutral surface are assumed to average out on a macroscopic scale. The justification of this is that regions of local variation, even if they are on the order of the diameter of the shot particle, are negligibly small in relation to the size of the plates considered. This is the same type of assumption made for all inhomogeneous materials such as concrete or crystalline metals if they are to be treated as a continuum. Effects of local variations are therefore neglected in the overall behavior of the part.

A thin plate that is uniformly peened on one side only, will be deformed in two ways. The plate will assume a curved shape due to the net bending moment on the cross section with the convex side of the plate oriented in the direction opposite the direction of the shot stream as shown in Figure 4. The resulting

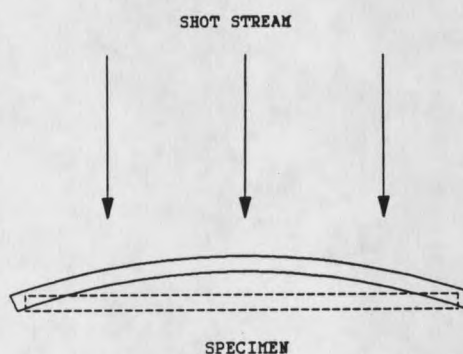


Figure 4. Curvature Development and Growth Due to Shot Peening.

curvature in peened specimens is seen to be somewhat uniform. In fact, reference [4] assumes the curvature to be constant thus providing an additional indication that local variations do not affect the large scale behavior of the plate.

In addition to curvature development, the overall length and width of the plate increase. This increase in dimension is termed "growth" in the aircraft industry. Growth is the same physical quantity as the average in-plane strain in the plate. The two effects

of growth and curvature are used to quantify the shot peening process.

The commonly accepted method for quantifying the shot peening process is called the Almen<sup>1</sup> test. The Almen test is performed on a small flat strip of spring steel of standard size and hardness by peening the strip uniformly on one side to saturation. During the test the specimen develops a convex curvature (See Figure 4). Saturation is said to have been reached when the arc height has attained a maximum value. The arc height, measured at saturation, has become a standard of measurement referred to as the "Almen arc height peening intensity." Details of the design and use of Almen gauges and test strips are given in Military Specification MIL-S-13165 [16] and in an SAE standard [17]. Reference [1] also describes the Almen test in some detail.

Several attempts have been made to relate the Almen peening intensity to the residual stress distribution and to the thickness of the plastically deformed layer,  $h_p$ . [6,7,9] Al-Hassani, [6], points out that the depth of the plastic layer is not uniquely determined by the saturation arc height of a peened Almen strip. The residual stress distribution is therefore not uniquely determined by the Almen peening intensity. The Almen test also does not quantify growth in any way.

#### Application to Commercial Aircraft Wing Skins

In the manufacture of commercial aircraft wing skins, large thin plates of aluminum are routinely peen formed to fit complex aerodynamic contours. Depending on the part, the alloy is usually 2024-T3 or 7075-T6. The plates generally have complicated boundaries

---

<sup>1</sup>. Named after John Otto Almen who, as a scientist with General Motors in the 1920's, invented the Almen test to provide a standard with which to measure the effects of shot peening.

and variable thickness. Thicknesses of 0.125 inches (0.318 cm) are typical but can vary anywhere from 0.08 inches (0.20 cm) to 0.5 inches (1.3 cm). Wing skins may vary in length from less than 30 feet (9.1 m) to more than 80 feet (24.4 m). The width may vary from approximately 3.5 feet (1.1 m) to 7 feet (2.1 m). [5] To achieve the desired contour the plate is shot peened in various nonuniform patterns that depend on the desired contour, the thickness variation, and the material properties of the plate. The peen forming process causes the plate to warp out-of-plane thereby producing the desired contour.

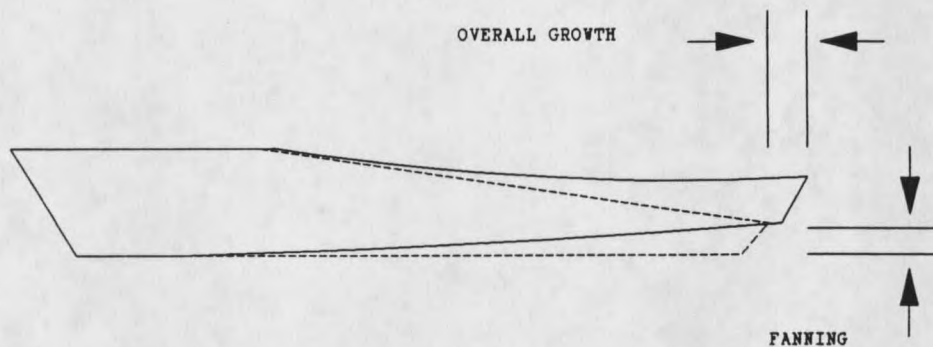


Figure 5. Fanning and Overall Growth.

In addition to out-of-plane displacements, peen forming produces in-plane displacements that must be considered. Two effects caused by in-plane displacements, known as overall growth and fanning, can have a substantial effect on the final shape of the wing skin. [5] The cumulative growth of the material from one end of the wing skin to the other can produce a substantial overall lengthening of the wing skin. Reference [5] suggests 0.25 inches in fifty feet (0.635 cm in 15.25 m) as typical. The magnitude of this typical value is confirmed in the results of this work. Overall growth of the wing skin in the chordwise direction is negligible due to the small width of the panels. Fanning is also caused by growth of the material but produces an angular rotation of part of the wing skin

as shown in Figure 5. Overall growth and fanning can cause certain features of the wing skin, such as stiffeners and holes, to move in the plane of the wing skin. These effects can also produce substantial distortion of the wing skin boundary. It is therefore desirable to control in-plane motions as well as the contour.

The peen forming process, as practiced at the Boeing Commercial Airplane Company, is applied in three stages with sanding and checking operations between stages. The three stages are spanwise peening, chordwise peening, and compression peening.

First the machined plate is passed through the spanwise peening machine. Spanwise peening is more intense than either chordwise or compression peening and is applied to both sides. As a result, the primary effect of spanwise peening is growth of the plate. Growth alone will not be effective in contour development in an initially flat plate. Curvature of the plate is necessary for growth to produce out-of-plane displacements.

The second stage of the process, chordwise peening, is primarily used for development of curvature of the plate. Chordwise peening is on the order of five times less intense than spanwise peening. Experimental work done at Boeing indicates that the growth due to chordwise peening is negligible. Since growth due to chordwise peening is neglected, the curvature is produced by peening only one side of the plate. The resultant bending moment on the cross section is therefore maximized. Also indicated was that when chordwise peening was applied in regions where spanwise peening had previously been applied, the additional peening had little effect on the deflection of the plate. Thus spanwise peening is applied with greater intensity on one side than the other to develop curvature in addition to growth. In regions where spanwise peening has not been applied curvature development is achieved with chordwise peening.

The third stage of the process, compression peening, is primarily a surface treatment to improve resistance to fatigue and corrosion. As such, it is applied uniformly to both sides of the plate. Compression peening is not intended for contour development although it does have a small effect on the final shape.

Successful peen forming of a wing skin depends on determining the relationship between an unknown shot peening intensity distribution or peening pattern, and the known plate geometry, material properties, and contour geometry. It appears that most work to date has been experimental in nature. Except for reference [10], very little has been found to indicate that numerical techniques such as the finite element method have been used to analyze the peen forming process. A method for calculating the surface force needed to achieve a given contour and a relationship between surface force and peening intensities is presented in reference [10]. Of all the references listed, this one has an objective similar to that of this work. The author of reference [10] has chosen the finite difference method for solving the differential equations that govern plate bending. The finite difference method is difficult to apply to complex geometries, boundary conditions, and contours. In addition, the method of determining peening patterns presented in reference [10] appears to involve peening on only one side of the plate. Also, in-plane displacements are not considered. It is strongly believed that the finite element approach is more easily applied to problems of a general nature.

Current methods of predicting peening patterns are approximate and depend to a large extent on the skill and experience of the peening equipment operator. These approximate methods are adequate for symmetric contours with relatively mild curvatures. Peening patterns necessary for highly curved or twisted contours, however, are not predicted well by current methods. In addition, it is known that substantially different peening

patterns may be used to produce the same contoured shape.

It is the purpose of this investigation to further the understanding of the peen forming process as applied to the large thin plates used in aircraft wing skins. A finite element approach is taken toward modeling the peen forming process. A general method of determining the optimal shot peening intensity pattern required to produce an arbitrary aerodynamic contour while controlling in-plane displacements is presented.

## CHAPTER II

## STRESS DISTRIBUTION ON THE CROSS SECTION

Residual stresses are also called self-equilibrating stresses because they are in static equilibrium with no external loads applied. Shot peening is a dynamic process and induces stresses in the material which are not in equilibrium initially. Static equilibrium is achieved after stresses due to the displacement of the material are sufficient to balance those caused by the peening action. Taking into account the assumptions of thin plate theory and the invariance of the in-plane stress as stated in Chapter I, there is only one independent stress component left to consider and it can be expressed as a scalar function of the depth and position on the plate. At this point a coordinate system is defined for the plate such that the  $x$  and  $y$  coordinates are in the plane of the plate and the  $z$  coordinate indicates the depth as shown in Figure 6. Figure 6 also shows a typical residual stress distribution for a thin plate uniformly peened on the top surface.

[6,7] Qualitatively, the stress distribution

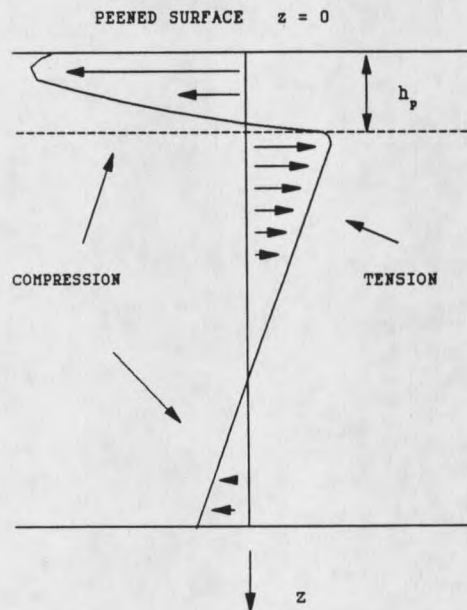


Figure 6. Typical Residual Stress in a Thin Plate.

of Figure 6 is generally accepted as correct and is supported by extensive experimental evidence. If the plate is not uniformly peened then Figure 6 represents the  $z$  variation of the residual stress at a specific point on the plate. In the discussion that follows, the stresses are considered to be the stresses evaluated at a specific point,  $(x,y)$ . They are therefore expressed as functions of  $z$  only.

It is assumed that the residual stress,  $\sigma(z)$ , can be decomposed into three components as follows:

$$\sigma(z) = \sigma_S(z) + \sigma_F(z) + \sigma_B(z). \quad (2)$$

$\sigma_S(z)$  is the initial nonequilibrium stress due to shot peening.  $\sigma_F(z)$  is an equilibrating elastic stress due to uniform stretching of the plate.  $\sigma_B(z)$  is an equilibrating elastic stress due to pure bending of the plate. It is further assumed that  $\sigma_S(z)$  is applied to the plate uniformly and instantaneously thereby neglecting the local nature of the plastic deformation. The assumption of uniformity of the initial stress is valid if the plate dimensions are much larger than the regions of local variation.

### Effects of Nonlinear Material Behavior

The assumption of no distortion of the cross section places restrictions on the form that the strain distribution can take. For plane stress, assuming  $\sigma_x = \sigma_y = \sigma$ , Hooke's law for an elastic material reduces to

$$\sigma(z) = E(z)\epsilon(z)/(1-\nu) \quad (3)$$

where  $\epsilon$  is the strain,  $E$  is the modulus of elasticity, and  $\nu$  is Poisson's Ratio. Determining the stress distribution through the entire thickness therefore requires knowledge of the material properties of both the elastic and plastic layers. If nonlinear material behavior

such as strain hardening of the plastic layer is accounted for, the elastic stress distributions,  $\sigma_F(z)$  and  $\sigma_B(z)$ , are necessarily nonlinear.

As an illustration of this, let Poisson's ratio be constant through the entire thickness and consider the modulus of elasticity to be a function of  $z$  given by:

$$E(z) = E[1+k(1-z/h_p)] \quad 0 \leq z \leq h_p \quad (4)$$

$$E(z) = E \quad h_p \leq z \leq h$$

where  $k$  is a strain hardening constant. This function is not intended to represent the effects of shot peening. It is intended only as an illustration of the effect of strain hardening of the plastic layer on the stress distribution when the condition of no distortion of the cross section is enforced.  $E(z)$  is a piecewise linear function as shown in Figure 7.

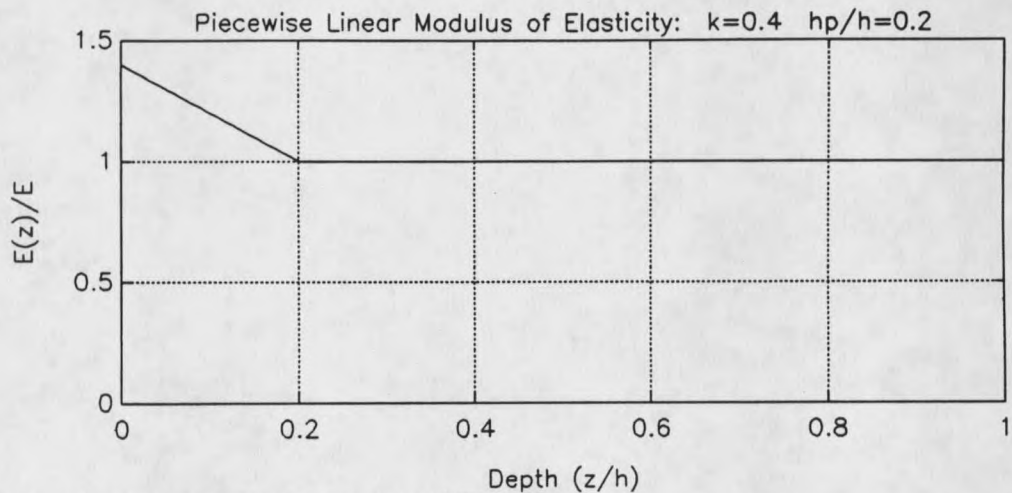


Figure 7. Piecewise Linear Modulus of Elasticity.

The stress distribution,  $\sigma_F(z)$ , corresponds to a constant strain through the thickness.

Combining equations (3) and (4) gives

$$\sigma_F(z) = E\epsilon[1+k(1-z/h_p)]/(1-\nu) \quad 0 \leq z \leq h_p \quad (5)$$

$$\sigma_F(z) = E\epsilon/(1-\nu) \quad h_p \leq z \leq h$$

In terms of the resultant force on the cross section, F,

$$\sigma_F(z) = -2F[1+k(1-z/h_p)]/(h_p k+2h) \quad 0 \leq z \leq h_p \quad (6)$$

$$\sigma_F(z) = -2F/(h_p k+2h) \quad h_p \leq z \leq h$$

where h is the plate thickness and

$$F = - \int_0^h \sigma_F(z) dz. \quad (7)$$

$\sigma_B(z)$  corresponds to a linearly varying strain distribution with zero strain at the neutral axis. This can be written as

$$\sigma_B(z) = E\epsilon[1+k(1-z/h_p)](z_n-z)/(1-\nu) \quad 0 \leq z \leq h_p \quad (8)$$

$$\sigma_B(z) = E\epsilon(z_n-z)/(1-\nu). \quad h_p \leq z \leq h$$

In terms of the resultant moment on the cross section, M,

$$\sigma_B(z) = -36M(h_p k+2h)[1+k(1-z/h_p)](z_n-z)/\alpha \quad 0 \leq z \leq h_p \quad (9)$$

$$\sigma_B(z) = -36M(h_p k+2h)(z_n-z)/\alpha \quad h_p \leq z \leq h$$

where

$$M = - \int_0^h \sigma_B(z) (z_n-z) dz \quad (10)$$

$$\alpha = h_p k(h_p^3+6h_p^2h-12h_p h^2+12h^3) + 6h^4 \quad (11)$$

and  $z_n$  is the z coordinate of the neutral axis.  $z_n$  is determined by requiring that  $\sigma_B(z)$  represent pure bending. Pure bending requires that  $\sigma_B(z)$  produce zero net force on the cross section or

$$0 = \int_0^h \sigma_B(z) dz. \quad (12)$$

Equation (12) yields

$$z_n = (h_p^2 k+3h^2)/(3h_p k+6h). \quad (13)$$

The elastic stresses given by equations (6) and (9) are clearly nonlinear. The normalized stresses,  $\sigma_F(z)(1-\nu)/E\epsilon$  and  $\sigma_B(z)(1-\nu)/E\epsilon h$ , are plotted in Figures 8 and 9.

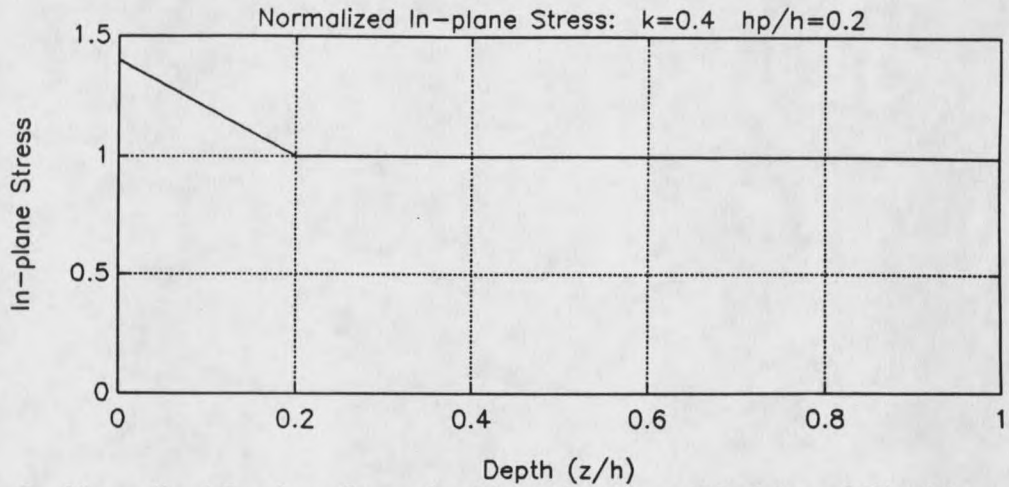


Figure 8. Normalized In-plane Stress for Piecewise Linear Modulus of Elasticity.

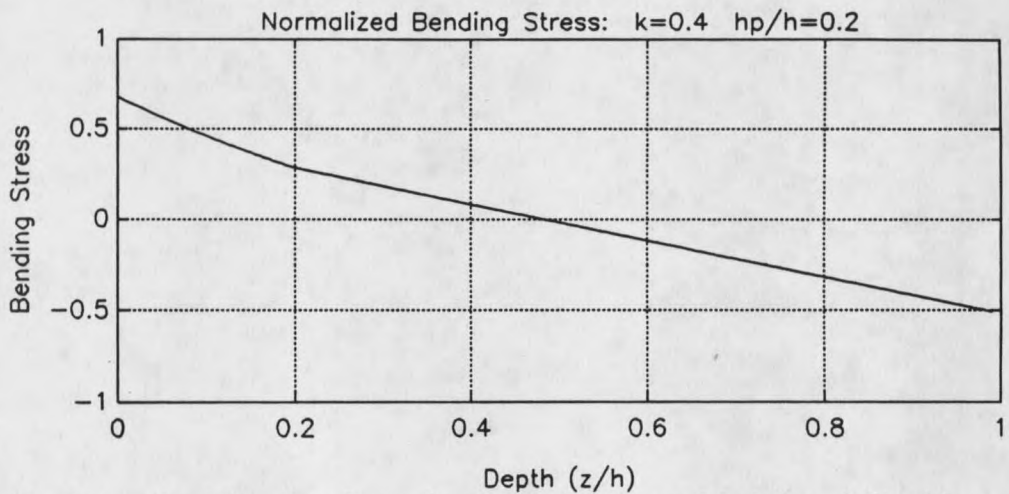


Figure 9. Normalized Bending Stress for Piecewise Linear Modulus of Elasticity.

The elastic unloading of the plate is a complicated nonlinear function of  $h_p$  and the strain hardening constant,  $k$ . Figures 8 and 9 indicate however that nonlinear material behavior of the cross section can be neglected if  $h_p$  is small compared to the thickness or

if the strain hardening constant is small. This assumption may produce inaccuracies if the peening intensity and material properties are such that  $h_p$  and strain hardening become significant. Such a condition is unlikely to exist in the peen forming of aircraft wing skins.

### Net Effect of the Initial Stress Distribution

Assuming constant material properties through the entire thickness, ( $k=0$  in the above example), equation (13) yields  $z_n = h/2$  and equations (6) and (9) give the following forms for  $\sigma_F(z)$  and  $\sigma_B(z)$ :

$$\sigma_F(z) = -F/h \quad (14)$$

$$\sigma_B(z) = -12M(h/2-z)/h^3. \quad (15)$$

The residual stress becomes

$$\sigma(z) = \sigma_S(z) - F/h - 12M(h/2-z)/h^3. \quad (16)$$

Neglecting body forces, the equilibrium equations for the cross section are

$$0 = \int_0^h \sigma(z) dz \quad (17)$$

$$0 = \int_0^h \sigma(z) (h/2-z) dz. \quad (18)$$

These equations must be satisfied at every point on the plate. Substituting equation (2) into equations (17) and (18), the equilibrium equations become

$$0 = \int_0^h [\sigma_S(z) + \sigma_F(z) + \sigma_B(z)] dz \quad (19)$$

$$0 = \int_0^h [\sigma_S(z) + \sigma_F(z) + \sigma_B(z)](h/2-z) dz. \quad (20)$$

Now substituting equations (7), (10), and (12) into equations (19) and (20), and noting that

a constant stress has zero moment about the neutral axis,  $z_n = h/2$ , the equilibrium equations become

$$0 = \int_0^h \sigma_S(z) dz - F \quad (21)$$

$$0 = \int_0^h \sigma_S(z)(h/2-z) dz - M. \quad (22)$$

Equations (21) and (22) indicate that the net effect of shot peening can be represented by the two stress resultants. The resultant force,  $F$ , corresponds to a simple stretching action and the resultant moment,  $M$ , corresponds to a simple bending action. If the peening is nonuniform so that  $\sigma_S$  is a function of  $x$  and  $y$  then  $F$  and  $M$  are also functions of  $x$  and  $y$ . Note that the sign convention requires a positive bending moment for tension on the top surface,  $z=0$ , (See Figure 6).

### Mathematical Forms for the Initial Stress Distribution

Unfortunately, an analytical form for the initial stress,  $\sigma_S(z)$ , is not known at present. References [6,7] present two formulations of the initial stress distribution. Each is discussed and some problems associated with each are addressed.

#### Spherical Cavity Model

Al-Hassani proposes the following initial stress distribution based on an analogy with the residual stress distribution in a spherical cavity model. [6,7]

$$\sigma_S(z) = Y\{1 - 2\ln[(h_p + R)/(z + R)] - \quad (23)$$

$$2[1 - (h_p + R)^3/(h + R)^3]/3\} \quad 0 \leq z \leq h_p$$

$$\sigma_S(z) = 2Y\{[(h + R)^3/(z + R)^3]/2 + 1\}[(h_p + R)^3/(h + R)^3]/3 \quad h_p \leq z \leq h$$

where  $R$  is the shot radius and  $Y$  is the yield stress of the material. The normalized initial stress,  $\sigma_S(z)/Y$ , is plotted in Figure 10 for  $h_p$  equal to 0.0, 0.05, ..., 0.3.

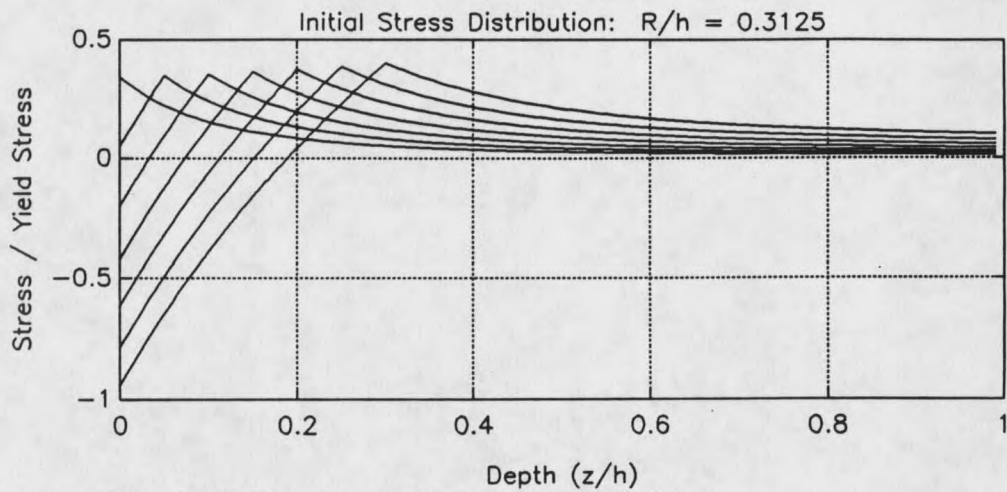


Figure 10. Initial Stress Based on Spherical Cavity Model.

Figure 10 illustrates two problems with this formulation of  $\sigma_S(z)$ . First, for small values of  $h_p$ ,  $\sigma_S(z)$  is tensile throughout the entire thickness. In fact, the limiting case of  $h_p = 0$  has a substantial tensile stress through the entire thickness when none should be present. Second, it is assumed that  $\sigma_S(z)$  is due to shot peening alone with no elastic deformation having taken place. By definition, the elastic region is stress free if no elastic deformation is present. Figure 10 indicates a tensile stress throughout the elastic region. If Hooke's law is applied to get the strain and the strain is then integrated to get the deformation, it follows that equation (23) implies the presence of an initial deformation in the elastic region. Furthermore, the deformation of the cross section is nonuniform.

Reference [6] performs the integrations for  $F$  and  $M$  in equations (21) and (22), however errors exist in the tabulated results. The correct results are

$$F = Y\{2R\ln(1+h_p/R) + (-9h_p+R)/6 + (3h-R)[(h_p+R)^3/(h+R)^3]/6\} \quad (24)$$

$$M = Y\{R(h+R)\ln(1+h_p/R) + h_p(2h_p-5h-6R)/6 + (h_p+R)(h-h_p)(h^2-3hh_p-2h_pR)/[12(h+R)^2]\}. \quad (25)$$

The stress resultants,  $F/Yh$  and  $M/Yh^2$ , are plotted as functions of  $h_p$  in Figures 11 and 12.

Figures 11 and 12 also indicate the previously mentioned problems when  $h_p$  is small. In particular, the resultant force plotted in Figure 11 is tensile for all values of  $h_p$  less than  $h/2$ . This means that the equilibrating stress is compressive, causing the part to shrink. Likewise, Figure 12 indicates that for values of  $h_p$  less than about  $0.17h$  the resultant moment is positive. The equilibrating moment is therefore negative causing the part to arc in the same direction as that of the shot stream. Both predictions are contrary to experimental evidence.

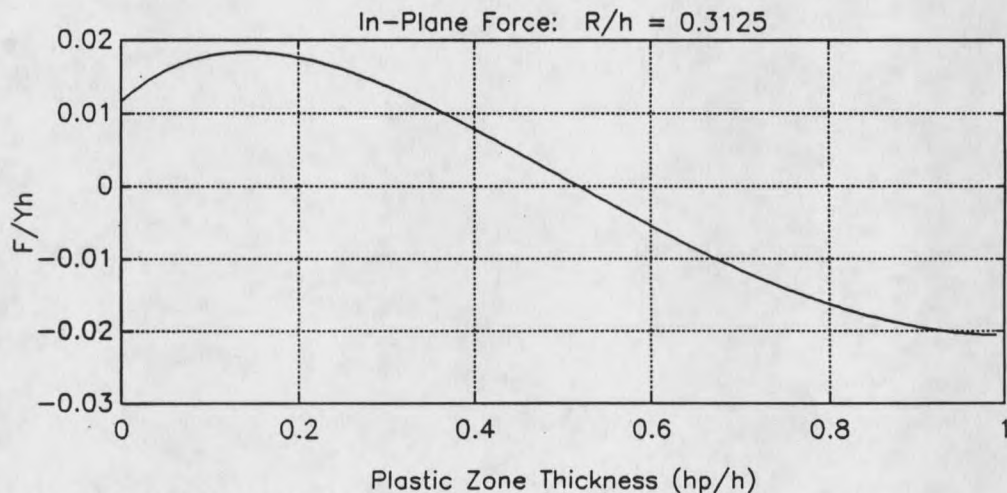


Figure 11. Normalized In-plane Stress Resultant.

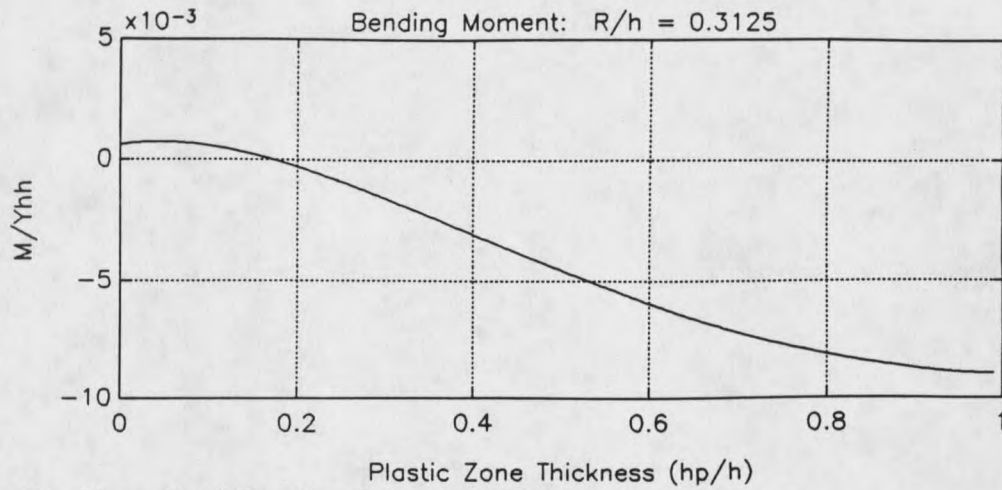


Figure 12. Normalized Bending Stress Resultant.

### Thick Section Empirical Model

Another form for the initial stress distribution presented in references [6,7] is proposed by Flavanot and Nikulari. It is an empirical relation based on the peening of very thick sections. Deflection of thick sections due to shot peening is negligible. The residual stress therefore does not include a substantial elastic stress component.  $\sigma_S(z)$  is given by

$$\sigma_S(z) = -E\epsilon_m \cos\left\{\frac{\pi}{2}\left[\frac{(z-\alpha h_p)}{(1-\alpha)h_p}\right]\right\}/(1-\nu) \quad 0 \leq z \leq h_p \quad (26)$$

$$\sigma_S(z) = 0 \quad h_p \leq z \leq h$$

where

$$\epsilon_m = 0.9Y(1-\alpha)^{1/2}/E \cos\left\{\frac{\pi}{2}\left[\frac{\alpha}{(1-\alpha)}\right]\right\} \quad (27)$$

$\alpha h_p$  = depth of the maximum compressive residual stress.

For soft materials such as aluminum the maximum compressive residual stress occurs at the surface. This requires that  $\alpha h_p$  and therefore  $\alpha$  equal zero. [6,7]  $\sigma_S(z)$  becomes

$$\sigma_S(z) = -0.9Y \cos\left[\frac{\pi}{2}\left(\frac{z}{h_p}\right)\right]/(1-\nu) \quad 0 \leq z \leq h_p \quad (28)$$

$$\sigma_S(z) = 0 \quad h_p \leq z \leq h$$

The normalized initial stress,  $\sigma_S(z)/Y$ , is plotted in Figure 13 for  $h_p$  equal to 0.0, 0.05, ..., 0.3.

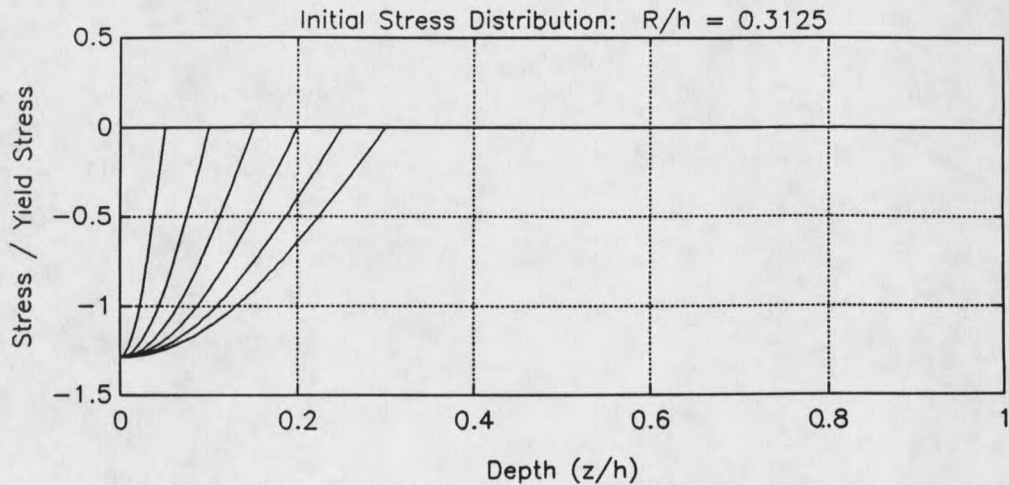


Figure 13. Initial Stress Based on Thick Section Empirical Model.

The stress distribution of Figure 13 indicates compression throughout the plastic layer and zero stress in the elastic layer. This formulation is intuitively more appealing than that of the spherical cavity model for several reasons. There is no initial deformation of the elastic layer. The stress in the plastic layer is compressive for all values of  $h_p$ . Finally, in the limiting case of  $h_p = 0$  the entire cross section is stress free. The maximum compressive stress is, however, substantially greater than the yield stress of the material. This result seems reasonable for a strain hardening material. References [1,2] however, state that the maximum compressive stress in the plastic layer is typically on the order of one half the yield strength of the material although no data is presented.

Equations (21) and (22) give the stress resultants

$$F = -1.8Yh_p/[\pi(1-\nu)] \quad (29)$$

$$M = 0.9Yh_p(2\pi h_p - 4h_p - \pi h)/[\pi^2(1-\nu)]. \quad (30)$$

The normalized stress resultants,  $F/Yh$  and  $M/Yh^2$ , are plotted as a function of  $h_p$  in Figures 14 and 15.

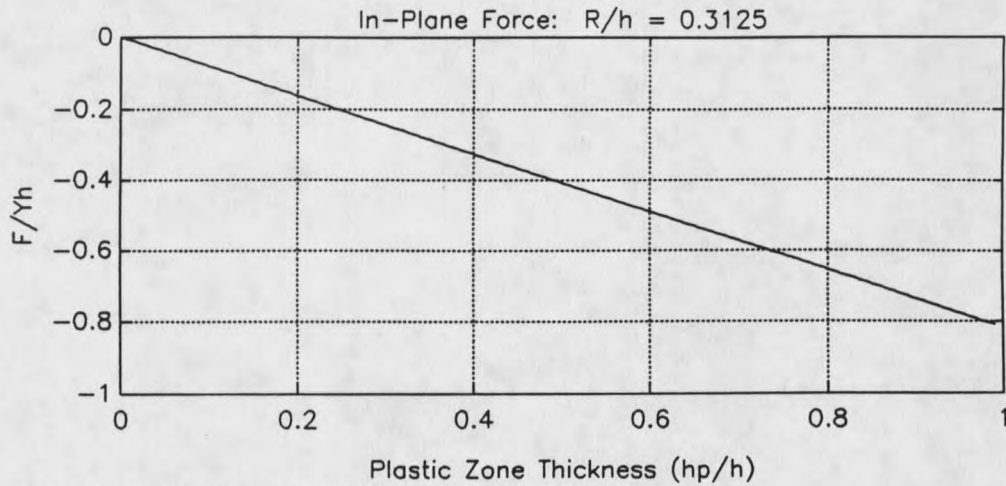


Figure 14. Normalized In-plane Stress Resultant.

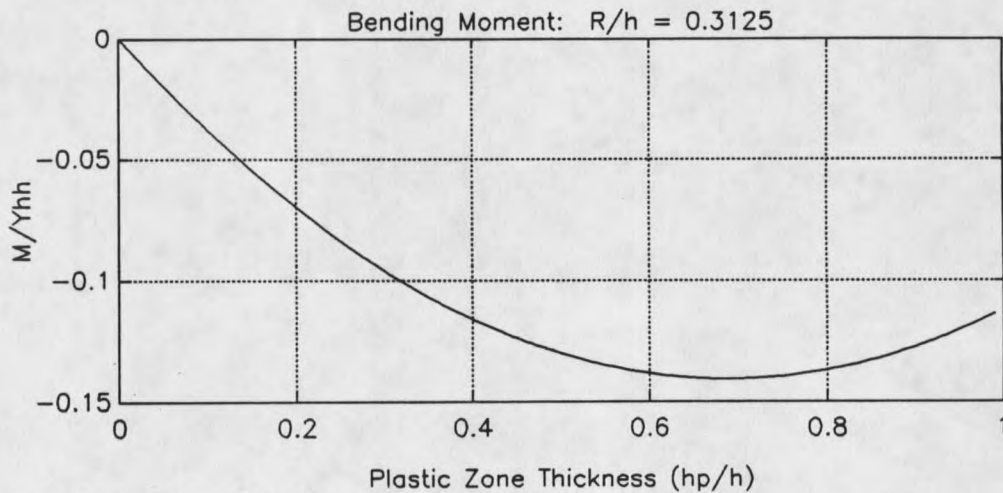


Figure 15. Normalized Bending Stress Resultant.

Both figures indicate negative stress resultants for all values of  $h_p$ . The equilibrating stresses are therefore positive corresponding to experimental results. Figure 15 also reveals another aspect of the shot peening process. The magnitude of the resultant moment on

the cross section increases to a maximum value as  $h_p$  increases to about  $0.7h$ . The magnitude of the resultant moment then begins to decrease. Maximum peening intensity, therefore, does not necessarily correspond to maximum bending. Figure 14, however, indicates that maximum peening intensity does correspond to maximum growth.

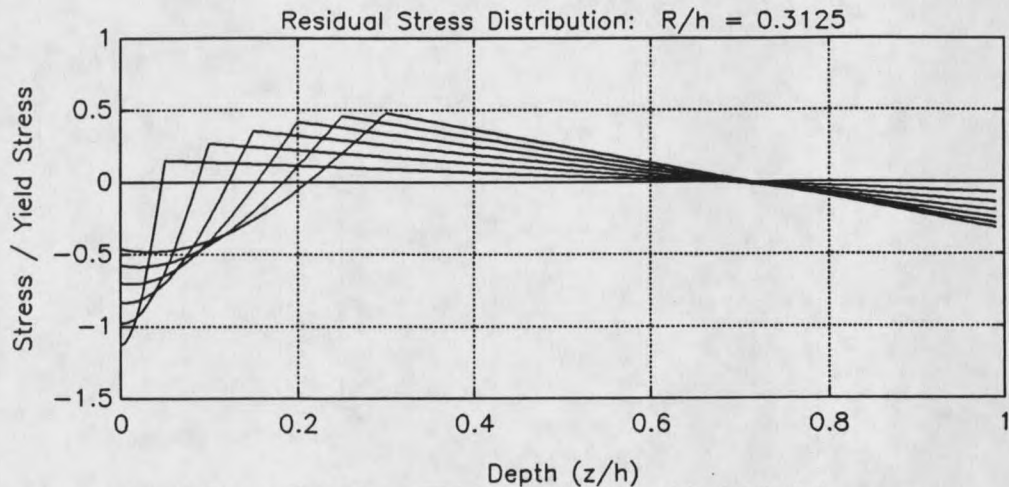


Figure 16. Residual Stress Based on Thick Section Empirical Model.

The residual stress,  $\sigma(z)/Y$ , is plotted in Figure 16 for  $h_p$  equal to 0.0, 0.05, ..., 0.3. Reference [7] states that plots of the residual stress distribution using the above formulation agree remarkably well with experiment although no plots are presented. Figure 16 indicates that for increasing values of  $h_p$  the maximum compressive residual stress decreases. This is a consequence of the fact that both elastic stresses are positive at the peened surface. When these positive stresses are added to the negative initial stress the magnitude of the residual stress is reduced. Reference [9] presents experimental data indicating that the maximum residual compressive stress increases with increasing air pressure. Since the air pressure in an air-type machine is directly related to the velocity of the shot, and in light of equation (1), this formulation presents a contradiction.

This discrepancy may be attributed to the fact that the stress and deflection history of the part has been ignored. In reality, the stress due to shot peening,  $\sigma_S(z)$  develops gradually in the presence of elastic stresses and deformations. References [1,2] state that the stress state of the part, as well as restraints on the parts movement during peening, can have a substantial effect on the resulting maximum compressive residual stress. This phenomenon can be explained by considering how the material yields. During the impact of a shot particle, the surface material yields in tension in the plane tangent to the surface. If tensile elastic stresses are present, the surface material will yield sooner allowing more plastic deformation to take place. If the elastic stresses are compressive, less plastic deformation will result. Since the maximum compressive residual stress is related to the amount of plastic deformation that has taken place, the presence of restraints necessarily has an effect on the resulting stress distribution.

### Conclusions

The spherical cavity formulation for  $\sigma_S(z)$  is not consistent with known effects of shot peening and experimental results. The discrepancies indicate that the current level of knowledge of the residual stress in a shot peened part is inadequate for quantitative analysis of the peen forming process. It is not within the scope of this work to address this problem and no attempt will be made to do so. Instead, empirical equations will be relied upon to provide the relationship between Almen peening intensity and the quantity of growth and curvature produced.

The thick section empirical model provides a more reasonable formulation of the residual stress distribution. This model does, however, predict larger maximum stresses than references [1,2]. This contradiction casts doubt on the validity of both the model and the

statements made in references [1,2].

In this work, empirical relations provided by The Boeing Company will be used. The equations are very specific and apply only to thin specimens of certain alloys used in wing skins. As such, these equations do not provide a general formulation for the stress distribution.

## CHAPTER III

## DEFLECTION CALCULATIONS

Before the peening pattern necessary to produce a given contour can be determined it is necessary to understand the response of a plate to an arbitrary peening pattern. The plates considered in this work generally have arbitrary boundaries, thickness variation, and desired contour. Furthermore, the thickness and desired contour are usually expressed in terms of numerical data rather than a continuous function. A numerical approach to the problem is therefore required.

The overall analysis method used in this work is the finite element method. There are several advantages of the finite element method over other numerical methods such as the finite difference method. The finite element method is widely used for structural analysis problems, including thin plate and shell structures. The method can be easily applied to problems with complex geometries and boundary conditions such as those associated with wing skins. Finally, there are many finite element software packages that are readily available. A number of these are in the public domain and can be modified fairly easily to model the peen forming process.

The finite element method is approximate as are all numerical methods. The differential equations that govern the response of a mechanical system to stimuli are reduced to a system of algebraic equations. The resulting equations relate a set of nodal loads, (stimuli), to a set of nodal displacements, (response). In matrix form the basic finite

element equation is written

$$\{F\} = [K] \{d\} \quad (31)$$

where

$\{F\}_{nx1}$  = vector of nodal loads

$\{d\}_{nx1}$  = vector of nodal displacements

$[K]_{n \times n}$  = matrix of stiffness coefficients

$n$  = 6 times the number of nodal points.

After constraints sufficient to prevent rigid body motion are applied, equation (31) can be solved for the displacements,  $\{d\}$ , in terms of the loading,  $\{F\}$ . The effects of gravity are not considered in this work so  $\{F\}$  does not include those effects.

Since the residual stress in the plate is self-equilibrating, and gravitational effects are not considered, the plate cannot exert a force on the supports if the supports are statically determinate. To ensure that no forces are exerted on the plate by the supports, the constraints are required to be statically determinant. This requirement guarantees that the response of the plate is due solely to effects of shot peening. With a set of statically determinate supports, there cannot be any unknown forces in equation (31). This requires that every force in the load vector,  $\{F\}$ , be related to peening intensities.

### Elastic Response in Terms of Peening Intensity

Following the development of Chapter II, the stress resultants of  $\sigma_S(z)$  are given by equations (21) and (22), respectively. The elastic response of the cross section is then given by equations (14) and (15). The fact that  $\sigma_S(z)$  is not known is not important if the two stress resultants,  $F$  and  $M$ , can be related directly to peening intensities.

Results of extensive experiments previously conducted at Boeing Airplane Company were made available for use in this work. The tests were conducted to determine the response of thin aluminum strips to the effects of shot peening. Response was considered to be the two quantities, growth, and radius of curvature. Each test strip had dimensions 18 x 3 inches (45.7 x 7.6 cm) and was of constant thickness. Specimens of a variety of alloys and thicknesses were uniformly peened for various values of the process variables. The resulting growth and radius of curvature of each specimen was then measured. In these tests, process variables included shot velocity, shot size, and percent coverage. The result was a data base from which empirical equations could be derived. The equations relate Almen peening intensities to growth, radius of curvature, and thickness of the specimen. Each of the empirical relations derived is specific to a particular alloy, shot size, and percent coverage. The equations are not listed in this work and will be generically referred to as

$$\text{growth} = \epsilon = g(i_g, h) \quad (32)$$

$$\text{radius} = r = r(i_r, h) \quad (33)$$

where  $i_g$  and  $i_r$  are Almen peening intensities and  $h$  is the specimen thickness. Once the growth and radius are known, the stress resultants can be calculated.

The membrane stress resultant,  $F$ , is determined by substituting equations (3) and (32) into equation (14) yielding

$$F = -Ehg(i_g, h)/(1-\nu). \quad (34)$$

The bending stress resultant,  $M$ , is determined by using the standard plate bending equations

$$M_x = -D(w_{xx} + \nu w_{yy}) \quad (35)$$

$$M_y = -D(w_{yy} + \nu w_{xx}) \quad (36)$$

$$M_{xy} = -D(1-\nu)w_{xy} \quad (37)$$

where

$$M_x = - \int_0^h \sigma_x(z) (h/2-z) dz \quad (38)$$

$$M_y = - \int_0^h \sigma_y(z) (h/2-z) dz \quad (39)$$

$$M_{xy} = - \int_0^h \sigma_{xy}(z) (h/2-z) dz \quad (40)$$

$$D = Eh^3/[12(1-\nu^2)]. \quad (41)$$

D is the plate flexural rigidity.  $M_x$  and  $M_y$  are the bending stress resultants about the x and y axes, respectively.  $M_{xy}$  is the shear stress resultant.  $w_{xx}$ ,  $w_{yy}$ , and  $w_{xy}$  are the second partial derivatives of the out-of-plane displacement, w, taken with respect to the x and y coordinates. Equations (35), (36), and (37) relate the bending and shear stress resultants to the second partial derivatives of the displacement assuming all second order effects are negligible. Effects of nonlinear material behavior are also assumed to be negligible.

### Second Order Effects

If equations (35), (36), and (37) are to be used to relate radius of curvature to M as given by equations (15) and (33), the question of whether the empirically determined radius of curvature includes second order effects must be addressed. Second order effects may include such variables as rolling direction, residual stresses in the specimen, and orientation of the specimen with respect to the shot stream. If second order effects are significant, the response of the specimen may not be due solely to effects of shot peening.

The empirical relations will then reflect effects other than those due to shot peening. The calculated elastic response of the specimen may then be inaccurate.

In Chapter II, for uniform peening, it was assumed that the stress was invariant under rotations in the x-y plane. This requires  $\sigma_x(z) = \sigma_y(z)$  and  $\sigma_{xy}(z) = 0$ . Equations (38), (39), and (40) then give  $M_x = M_y = M$  and  $M_{xy} = 0$ . These are substituted into equations (35), (36), and (37) resulting in the requirements that

$$w_{xx} = w_{yy} \quad (42)$$

$$w_{xy} = 0. \quad (43)$$

For small slopes the second derivatives in equation (42) are approximately equal to the reciprocals of the radii of curvature. Equation (42) then requires

$$r_x = r_y \quad (44)$$

This result is substantiated by experimental results presented in reference [4]. These experiments were also conducted at The Boeing Company. A number of specimens of constant thickness were uniformly peened and the radii of curvature in the two principle directions, x and y, were measured. Results indicated that specimens with length to width ratios greater than four had essentially the same curvature in both principle directions. Also indicated was that these specimens were insensitive to orientation with respect to the rolling direction of the plate. Specimens of L/W less than two showed significant differences in radii of curvature indicating that second order effects were present. The specimens used in developing equations (32) and (33) had L/W equal to six. The assumption that second order effects are not included in equations (32) and (33) is therefore accepted in this work. In addition, no mention is made of twisting in any uniformly peened specimens so the assumption of no second order twisting effects is accepted as well.

Having assumed small slopes and that significant second order effects are not present in equation (33),  $M$  can now be related to the radius of curvature,  $r$ . Substituting equation (41) into equation (35) and letting  $M_x = M$  and  $w_{xx} = w_{yy} = 1/r(i_r, h)$  gives  $M$  as

$$M = -Eh^3/[12(1-\nu)r(i_r, h)]. \quad (45)$$

Substituting equations (34) and (45) into equations (14) and (15) gives the elastic response of the specimens directly in terms of Almen peening intensities:

$$\sigma_F(z) = Eg(i_g, h)/(1-\nu) \quad (46)$$

$$\sigma_B(z) = E(h/2-z)/[(1-\nu)r(i_r, h)]. \quad (47)$$

Equations (46) and (47) contain the empirically derived values of growth and radius of curvature. Effects of nonlinear material behavior of the cross section and the stress history of the specimen are therefore included. The main assumption inherent in these equations is that significant second order effects were not present in the data used to develop equations (32) and (33).

#### Finite Element Modeling of Shot Peening

At this point an analogy between the effects of shot peening a test specimen and the response of a test specimen to thermal loading may be drawn. Equation (46) represents a uniform in-plane expansion for a particular Almen peening intensity. This is analogous to a uniform thermal expansion brought about by a uniform temperature increase in the specimen. Likewise, equation (47) represents a uniform bending for a particular Almen peening intensity. This loading is analogous to a uniform bending brought about by a uniform temperature gradient through the thickness of the specimen. The loading due

to shot peening can therefore be modeled as a thermal loading. Denoting  $\sigma_F(0)$  and  $\sigma_B(0)$  by  $\sigma_{F0}$  and  $\sigma_{B0}$ , the Almen peening intensities can be thought of as analogous to thermal "stress intensities." In terms of growth, radius of curvature, and material properties, the stress intensities are

$$\sigma_{F0} = E g(i_g, h) / (1 - \nu) \quad (48)$$

$$\sigma_{B0} = E h / [2(1 - \nu) r(i_r, h)]. \quad (49)$$

Each element has one stress intensity related to expansion and one related to bending. Thermal problems of this nature are routinely solved using the finite element method.

The remaining problem of determining the components of  $\{F\}$  is reduced to integrating equations (46) and (47) over the element volume to get the element nodal loads, and through the assembly process, calculating the components of  $\{F\}$ . Figure 17 shows the

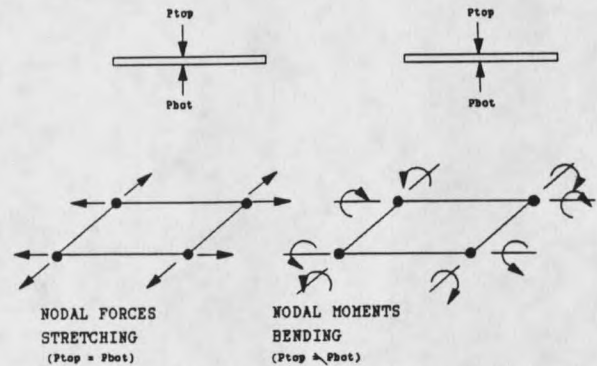


Figure 17. Nodal Equivalent Loads Due to Shot Peening.

element nodal loads for the two cases of growth and bending. The nodal loads are also referred to as nodal equivalent loads. They are the set of nodal loads having an effect equivalent to that of the shot peening effect.

### Effects of the Assembly Process

The method for calculating the elements of  $\{F\}$  outlined in the preceding paragraphs is intuitively appealing because the element nodal equivalent loads are directly related to Almen peening intensities. The element forces are simply summed according to Newton's second law during assembly to get the structure nodal equivalent loads. The

assembly process however, in addition to enforcing static equilibrium at the nodes, also enforces compatibility of displacements at the nodes. The compatibility requirement represents a constraint on the deflections of the model that was not present during the development of equations (32) and (33). This raises the question whether equations (32) and (33) apply to the peening of large plates.

Equations (32) and (33), as well as the results presented in reference [4], are based on the peening of unrestrained specimens. The element nodal equivalent loads are therefore equivalent to unrestrained peening of the element. In reality, only a relatively small region of a wing skin is being peened at any one time. This region is elastically restrained by the surrounding material during the process. In the assembled finite element model each nodal degree of freedom has a stiffness coefficient that is a combination of the stiffness of all of the surrounding elements. In a mathematical sense, a particular element in the model is therefore elastically restrained at the nodes by the surrounding elements. This suggests that nodal equivalent loads based on equations (32) and (33) cannot be directly transferred to the assembled structure. In this work equations (32) and (33) are assumed to apply recognizing that this may introduce some error into the analysis for contours requiring excessive growth or curvature. The claim that the stress and deflection history of the specimen is accurately represented also can no longer be made.

In addition to the above simplifications, an assumption regarding the element thicknesses must be made. Equations (32) and (33) are based on the peening of specimens of constant thickness. Wing skins however, are of variable thickness. Proper use of equations (32) and (33) would require that the elements be of constant thickness. This, however, would lead to less accurate modeling of the plate stiffness. In a typical wing skin the thickness variation is small except near some of the boundaries where the skin is

joined to an adjacent skin. In this work, the elements used are of variable thickness to more accurately model the plate stiffness. It is assumed that the slight variation in thickness over a single element will have a negligible effect on the nodal equivalent loads. A refined finite element mesh will not only improve the accuracy of the stiffness matrix but will also reduce the error incurred in using elements of variable thickness since the thickness variation over smaller elements is reduced.

### Nonlinear Considerations

The stiffness matrix,  $[K]$ , and load vector,  $\{F\}$ , in equation (31) are functions of the deflection of the plate. This makes equation (31) nonlinear. To perform the most accurate analysis, the actual geometry should be updated as the plate deforms during the simulated peening process. To do this requires knowledge of the peening pattern as well as the sequences in which peening is applied. In practice, the process is completed in stages as explained in Chapter I. In addition, each stage of the process involves numerous passes through the peening machines with different regions being peened on each pass. A nonlinear analysis of the deflection is only possible given a specific peening pattern and peening history. Since the ultimate goal is to determine the peening pattern necessary to produce a given final geometry, a nonlinear analysis becomes intractable.

In performing a linear analysis of a structure, the stiffness,  $[K]$ , and the load vector,  $\{F\}$ , are calculated only once. These calculations are usually based on the initial geometry of the structure. It is assumed that the structure undergoes small deflections so that the stiffness and load vector do not change significantly as the structure deforms. The initial geometry is used because the deformed geometry is generally not known. In the peening problem, however, the desired final geometry is known allowing the plate stiffness to be

calculated in the final configuration. Experience correlating results in which  $[K]$  and  $\{F\}$  were based on both initial, (flat), and final contour geometries indicates the final geometry can be used to get a reasonable approximation of the plate stiffness for the entire history of the peening process. Experience with wing skins indicates that the stiffness is not very sensitive to changes in geometry however, the load vector is. If the undeformed or flat configuration is used to calculate the load vector, serious errors can arise. This is best seen by considering the effects of a uniform in-plane stress resultant as shown in Figure 17. If the skin is considered to be flat then the nodal equivalent loads are parallel to the plane of the plate. This results in in-plane displacements with no out-of-plane motion. If the skin is deformed, however, there is a component of the in-plane force in the z-direction. This allows out-of-plane motion to take place. Since the growth effect of shot peening is known to produce substantial out-of-plane displacements, the final configuration is used for stiffness and load vector calculations.

### Software

The software used for this work is a linear finite element analysis program based on the SAP (Structural Analysis Program) series of programs developed at the University of California at Berkeley, specifically, SAP5 version 2. [18] The software was developed by tailoring SAP for the shot peening problem. With only minor exception, the original SAP code was unchanged. The software was streamlined by taking out all the dynamic analysis capabilities and all the element types except the plate/shell element. The solution routines were also streamlined to accommodate problems requiring a large number of load cases.

## CHAPTER IV

## PEENING INTENSITY PATTERN CALCULATIONS

Presently, the method used at the Boeing Company for calculating the peening intensity distribution required to produce a given contour is approximate. The method is geometric in nature and is based on simplifying assumptions which are not valid for complex contours. The objective of this work, therefore, is to develop a new technique for calculation of peening intensities which will be valid for general contoured shapes. In this chapter a summary of the geometric method currently used at Boeing is presented and some theoretical problems are identified. An alternate method based on the finite element method is then proposed.

Geometric Method

Equations (32) and (33) can be inverted to give the Almen peening intensities in terms of growth, radius of curvature, and thickness. The resulting equations are

$$i_g = i_g(\epsilon, h) \quad (50)$$

$$i_r = i_r(r, h). \quad (51)$$

The thickness,  $h$ , of the plate at any point is given in the design specifications. The problem of determining the Almen peening intensities is therefore reduced to calculating the desired growth and radius of curvature at each point on the wing skin. The desired

growth and radius of curvature are determined geometrically from the desired contour data. These quantities are then substituted into equations (50) and (51) for the Almen intensities.

Figure 18 shows a saddle shaped contour typical of that desired for many aircraft wing skins. In the discussion that follows,  $h$  denotes the chord height as shown rather than the thickness of the plate.  $R_s$  and  $R_c$  are the radii of curvature in the spanwise and chordwise directions, respectively. The center of the plate where  $R_s$  is measured is defined to be the "neutral axis." The chord height,  $h$ ,

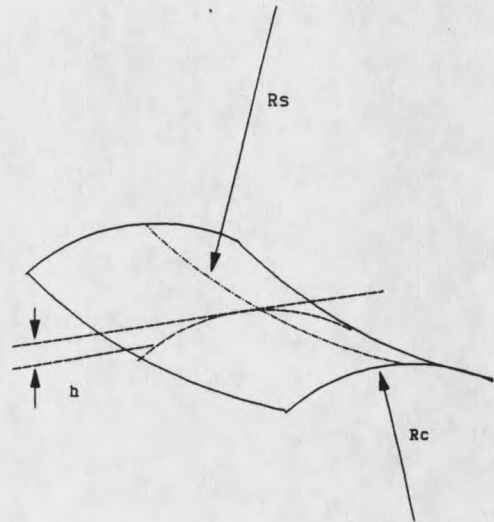


Figure 18. General Saddle Contour Geometry.

is measured vertically downward from the neutral axis. Note that the contour of Figure 18 is symmetric in the sense that the normal direction to the surface at the neutral axis is always in the same plane, i.e. the contour is not twisted about the neutral axis. The geometric quantities  $R_c$ ,  $R_s$ , and  $h$  at any point on the wing skin can be determined numerically from the  $x$ ,  $y$ , and  $z$  coordinates contained in the desired contour data. The quantities of growth,  $\epsilon$ , and radius of curvature,  $r$ , are calculated from  $R_c$ ,  $R_s$ , and  $h$ .

#### Theoretical Problems with the Geometric Method

Four sources of error are identified which are believed to be the major causes of inaccuracy in the geometric method. These are the measurements of  $R_s$  which affect the calculation of  $\epsilon$ , arbitrary definition of the neutral axis, neglect of coupling between the

effects of the chordwise and spanwise peening stages, and improper application of equations (50) and (51) to the wing skin.

Calculation of  $\epsilon$ . The amount of growth necessary at a given point on the contour is calculated as shown in Figure 19.  $L$  is the length of a material "fiber" measured along the curve of the neutral axis and  $\Delta L$  is the amount of elongation that is required at some point away from the neutral axis in the chordwise direction.

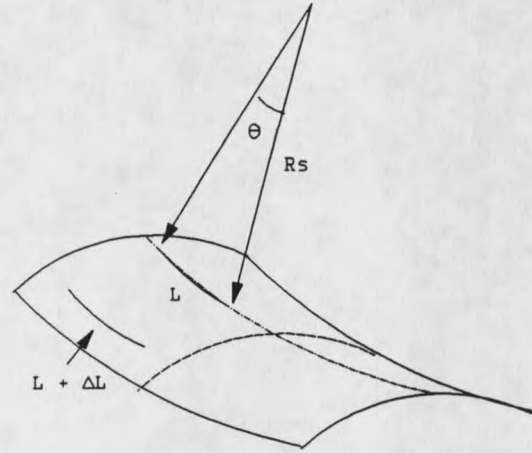


Figure 19. Calculation of Required Growth - Geometric Method.

The rationale is that in the undeformed configuration the length of both lines is

the same. After deformation the lines become curves on the contour. The growth of the material along the neutral axis is assumed to be zero while the growth of the material at points away from the neutral axis is given by

$$\epsilon = g = \Delta L/L \quad (52)$$

For  $\theta$  small, these curves are approximated by circular arcs and can be written

$$L = R_s \theta \quad (53)$$

where  $\theta$  is the angle subtended by the arc as shown. The growth can now be calculated by substituting equation (53) into equation (52) and expanding the result.

$$g = \Delta L/L \quad (52)$$

$$= \Delta(R_s \theta)/(R_s \theta)$$

$$g = (\theta \Delta R_s + R_s \Delta \theta)/(R_s \theta)$$

$$\begin{aligned}
 g &= (\theta \Delta R_s + R_s \Delta \theta) / (R_s \theta) \\
 &= \Delta R_s / R_s + \Delta \theta / \theta.
 \end{aligned}
 \tag{54}$$

At any particular cross section  $\theta$  is constant so the term  $\Delta \theta / \theta$  is zero. Equation (54) reduces to

$$g = \Delta R_s / R_s. \tag{55}$$

If  $R_s$  is always measured in the direction normal to the plate at the neutral axis then  $\Delta R_s$  is just the chord height,  $h$ . Equation (55) becomes

$$\epsilon = g = h / R_s \tag{56}$$

which is the equation used to calculate the desired growth.

There are some implicit assumptions being made in this calculation. The spanwise radius is always measured at the neutral axis. The actual radius is assumed to be

$$R_{\text{actual}} = R_s + \Delta R_s = R_s + h. \tag{57}$$

The actual spanwise radius at a point must be measured in the direction normal to the surface at that point as shown in Figure 20. In that case, the chord height,  $h$ , does not enter into the calculation of required growth.

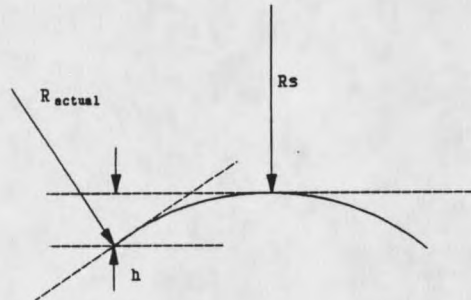


Figure 20. Actual Spanwise Radius at a Point Away from the Neutral Axis.

Definition of the Neutral Axis. Secondly, there is an assumption that the neutral axis follows a straight path down the center of the contour. Noting the definition of  $h$ , and in light of equation (56), it is seen that by defining a neutral axis, the strain along the

neutral axis must be zero. This is a geometric restriction on the strain field in the plate that is completely arbitrary. A strain field calculated using this method may not satisfy the governing differential equations for the plate. In fact, they are not considered at all. Also, only growth in the spanwise direction is considered.

The fact the governing differential equations are not considered in this method does not mean that they will not be satisfied. Since a wing skin is an actual physical system, the actual strain field must satisfy the governing equations. The actual strain field produced however, may be different than that calculated using the geometric method.

In addition to the existence of a neutral axis, the orientation of the neutral axis has an effect on the results. The chord height depends only on the chordwise curvature and the distance from the neutral axis. The calculated growth requirement is therefore based only on the spanwise and chordwise curvatures. For a general two dimensional surface the curvature has three independent components. In addition to the curvature in both the spanwise and chordwise directions, there is a component of curvature related to the twist about the neutral axis. This is seen by considering the second derivative of a function of two variables,  $z = f(x,y)$ . The second derivative of  $f(x,y)$ , denoted by  $D^{(2)}f$ , is a linear mapping that can be represented by a 2x2 matrix of the second partial derivatives.

$$D^{(2)}f = \begin{bmatrix} f_{xx} & f_{xy} \\ f_{yx} & f_{yy} \end{bmatrix} \quad (58)$$

If the spanwise and chordwise directions are  $x$  and  $y$ , respectively, then assuming small slopes, the radii of curvature are given by

$$f_{xx} = 1/R_s \quad (59)$$

$$f_{yy} = 1/R_c$$

The component,  $f_{xy}$ , is not considered in this method.

As an illustration of the error that can occur by neglecting  $f_{xy}$ , consider the spiral contour shown in Figure 21. This surface is given by  $z = f(x,y) = xy$ . The three independent components of the second derivative are

$$f_{xx} = 0$$

$$f_{xy} = 1$$

$$f_{yy} = 0.$$

Equations (59) then require the radii of curvature,  $R_s$  and  $R_c$ , to be infinite, the same as a flat plate. The contour generated with  $f(x,y) = xy$  has no chordwise or spanwise curvature, only a twist. The geometric method does not predict any peening for this contour because there is an implicit assumption of zero twist. As a consequence, the geometric method applied to a twisted contour gives inaccurate results.

Now consider the same contour given above expressed in a  $u-v$  coordinate system that is rotated by an angle  $\theta$  in relation to the  $x-y$  coordinate system as shown in Figure 22. The transformation equations from  $u-v$  coordinates to  $x-y$  coordinates are

$$x = u \cos\theta - v \sin\theta \tag{60}$$

$$y = u \sin\theta + v \cos\theta. \tag{61}$$

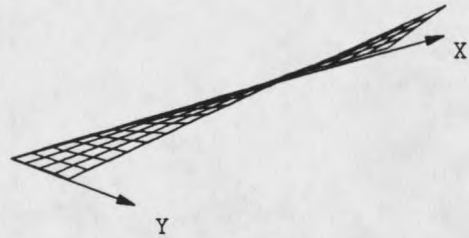


Figure 21. Twisted Contour.

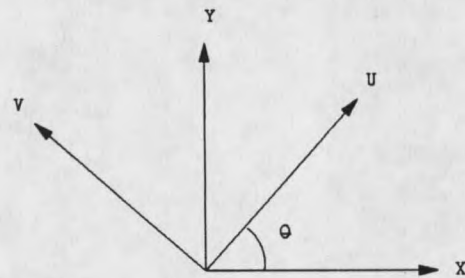


Figure 22. Rotated Coordinate System.

The function  $f(x,y) = xy$  becomes

$$\begin{aligned} f^*(u,v) &= f(x(u,v),y(u,v)) \\ &= (u \cos\theta - v \sin\theta)(u \sin\theta + v \cos\theta) \\ f^*(u,v) &= (u^2 - v^2) \sin(2\theta)/2 + uv \cos(2\theta). \end{aligned} \quad (62)$$

The three independent components of the second derivative are

$$\begin{aligned} f^*_{uu} &= \sin(2\theta) \\ f^*_{uv} &= \cos(2\theta) \\ f^*_{vv} &= -\sin(2\theta). \end{aligned} \quad (63)$$

If, for example,  $\theta = \pi/4$ , then equations (63) give

$$\begin{aligned} f^*_{uu} &= 1 \\ f^*_{uv} &= 0 \\ f^*_{vv} &= -1. \end{aligned} \quad (64)$$

If the neutral axis is then chosen so that it is parallel to the  $u$  direction, the spanwise radii of curvature,  $R_s$  and  $R_c$ , become 1 and -1, respectively, with no twist present. The radii of curvature and the necessary growth are thus dependent on the choice of coordinate system. This is clearly impossible for a physical system.

Coupling Between Chordwise and Spanwise Peening. Calculation of  $r$  for use in equation (51) is equally arbitrary. Since the chordwise peening stage is thought to have the greatest effect on chordwise curvature development, the radius of curvature,  $r$ , is taken to be the radius of curvature in the chordwise direction,  $R_c$ . This neglects any effect of the chordwise peening stage on the development of curvature in the spanwise direction. Effects of spanwise peening on curvature development in the chordwise direction are also neglected.

Application of Empirical Equations. Finally, the use of equations (32) and (33) and their inverses, equations (50) and (51), are based on the uniform peening of unrestrained specimens. They do not necessarily apply to the wing skin which is peened in a nonuniform manner. In addition to the problems discussed in Chapter III regarding equations (32) and (33), using a geometric method such as the one just described introduces another source of error.

The peening intensity distribution is not required to be continuous over the entire plate. In fact, due to limited machine precision and the fact that nonuniform peening is applied, the peening intensity distribution is only piecewise continuous. Figure 23 shows the boundary

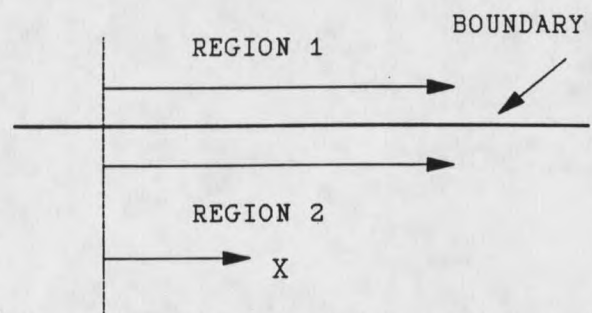


Figure 23. Boundary between Regions of Different Peening Intensity.

between two regions of a plate that have been peened with different intensities. The arrows on each side of the boundary indicate paths of integration. The slope and displacement of the surface are required to be continuous in every direction at the boundary between the two regions. On each side of the boundary, in the direction parallel to it, the radius of curvature and the growth can be integrated to get the slope and displacement, respectively. As the two paths are taken to be arbitrarily close to the boundary, continuity requires the growth on each side of the boundary to be equal. The two radii of curvature are likewise required to be equal. If these quantities are then used in equations (50) and (51) and assuming constant thickness across the boundary, the resulting peening intensities must be equal. The assumption that the two regions are peened with different intensities therefore leads to a contradiction. The fallacy lies in

assuming that the growth and radius of curvature found at some point on a nonuniformly peened contour are the same as the growth and radius of curvature found on an unrestrained peening specimen that has been peened with the same intensity. Due to the restraining effect of adjacent regions, they are not. Equations (32), (33), (50), and (51) are therefore used improperly with the geometric method.

Although there may be other sources of inaccuracy in the method, the most prominent ones have been illustrated.

### Practical Considerations

A final note on accuracy involves machine precision. This is a practical rather than a theoretical problem that will have an impact regardless of the method used to determine the peening pattern. The chordwise peening machine can be precisely controlled to within an 18" x 18" square grid and its heads are stationary. The spanwise peening machine can peen 18" x 3" regions precisely and has moveable heads. These limitations in machine precision will limit the accuracy of the contour. It is possible that the required degree of accuracy for some contours may require more precise application of shot peening than is possible using currently available machines.

### Finite Element Based Method

To avoid the problems outlined in the previous section with the empirical relations, equations (32), (33), (50), and (51), the method of calculating nodal equivalent loads presented in Chapter III is adopted. The approximations discussed in Chapter III remain, however the empirical relations are no longer applied to nonuniformly peened regions.

For simplicity in the discussion that follows, the initial stress intensities,  $\sigma_{F0}$  and  $\sigma_{B0}$  will be referred to simply as stress intensities.

If the displacement vector,  $\{d\}$ , can be expressed in terms of the stress intensities in each element then equations (49) and (50) are readily inverted to get the necessary growth and radius of curvature.

$$\epsilon = \sigma_{F0}(1-\nu)/E \quad (65)$$

$$r = Eh/2(1-\nu)\sigma_{B0} \quad (66)$$

Equations (65) and (66) represent the growth and radius of curvature that develop in an unrestrained element due to the stress intensities,  $\sigma_{F0}$  and  $\sigma_{B0}$ . The values of growth and radius of curvature are then based on the stresses in the elements rather than the geometry of the contour. The governing differential equations will then be satisfied to within the finite element approximation. Once the required growth and radius of curvature for each element are obtained, equations (50) and (51) are used to calculate the two Almen peening intensities for each element.

#### Displacements Due to Stress Intensities

The displacement of the plate in terms of the load vector is found by inverting equation (32).

$$\{d\} = [K]^{-1} \{F\} \quad (67)$$

Since equation (32) was assumed to be linear, the load vector,  $\{F\}$ , can be decomposed into a combination of separate load cases. In the peening problem each load case is taken to be the set of nodal equivalent loads corresponding to each stress intensity set equal to one with the rest set to zero. These form a linearly independent set of load cases from which all possible peening patterns may be constructed. The displacement vector,  $\{d\}$ , can then

be written as a linear combination of displacement cases, each due to a separate load case. The displacement cases are also linearly independent.

The total displacement can be written in matrix form,

$$\{d\} = [D]\{\sigma\} \quad (68)$$

where  $\{\sigma\}$  is the vector of stress intensities and  $[D]$  is a linear operator that maps the stress intensities into displacements. Each column of  $[D]$  represents a displacement case due to a single unit stress intensity and is calculated by the finite element method outlined in Chapter III. After all load cases and corresponding displacements are calculated, all of the elements of  $[D]$  are known. Note that the number of columns of  $[D]$  is equal to two times the number of elements in the finite element model and the number of rows of  $[D]$  is equal to six times the number of nodes. This is a consequence of the constraints placed on the individual load cases. Since the initial stresses, (both bending and membrane), are assumed to be invariant under rotations in the x-y plane, the load cases are restricted to those that are equivalent to this type of stress field. Therefore, for each element, only two independent stress intensities, one bending and one membrane, may be specified. This results in only two independent load cases per element. Each node has six degrees of freedom yielding six independent displacement components for each node. Assuming all of the displacements are given, equation (68) becomes an equation relating  $m$  known quantities (displacements) to  $n$  unknown quantities (stress intensities) where  $m$  equals six times the number of nodes and  $n$  equals two times the number of elements. The value of  $m$  is greater than that of  $n$  for all finite element meshes. Equation (68) is therefore noninvertible. This means that an arbitrary set of displacements,  $\{d_0\}$ , may not satisfy equation (68) which implies that an arbitrary contoured shape, in general, cannot be produced by shot peening. An approximate solution is therefore desired.

### Approximate Solution

Given an arbitrary set of desired displacements,  $\{d_0\}$ , a set of displacements,  $\{d\}$ , can be found that approximate  $\{d_0\}$  by minimizing the difference  $\{d\} - \{d_0\}$ . A scalar error function,  $f(\{d\}, \{d_0\})$ , is defined as the square of the length of the vector  $\{d\} - \{d_0\}$ .

The error function can be written in matrix form as

$$f = (\{d\} - \{d_0\})^T (\{d\} - \{d_0\}). \quad (69)$$

Substituting equation (68) into equation (69) gives

$$f = ([D]\{\sigma\} - \{d_0\})^T ([D]\{\sigma\} - \{d_0\}). \quad (70)$$

To find the set of stress intensities corresponding to a minimum value of  $f$ , the derivative of  $f$  with respect to the stress intensities is set equal to zero. The derivative of  $f$  is

$$df/d\{\sigma\} = 2[D]^T([D]\{\sigma\} - \{d_0\}). \quad (71)$$

Setting equation (71) equal to zero yields the following equation for the stress intensities.

$$[A]\{\sigma\} = \{b\} \quad (72)$$

where

$$\begin{aligned} [A] &= [D]^T[D] \\ \{b\} &= [D]^T\{d_0\}. \end{aligned}$$

The coefficient matrix,  $[A]$ , is symmetric and positive definite. Equation (72) therefore has a unique solution given by

$$\{\sigma\} = [A]^{-1}\{b\}. \quad (73)$$

The second derivative of  $f$  is

$$d^2f/d\{\sigma\}^2 = 2[D]^T[D] = 2[A]. \quad (74)$$

Since  $[A]$  is positive definite,  $\{\sigma\}$  represents a local minimum of  $f$ .

Substituting equation (73) into equation (68) and noting that  $\{b\} = [D]^T\{d_0\}$ , a set of displacements may be calculated that approximate the set of desired displacements in the

sense that the length of the vector  $\{d\} - \{d_0\}$  is a minimum.

$$\{d\} = [D][A]^{-1}[D]^T\{d_0\} \quad (75)$$

### Constraints on the Stress Intensities

The stress intensities given by equation (73) may not be realistic if their magnitudes exceed the capabilities of the peening machines. Also, the initial membrane stress intensities must be greater than zero since shot peening cannot have the effect of negative growth in an element. To allow for the possibility of enforcing a constraint on the magnitude of the stresses, an additional term is added to the error function that reflects their magnitudes. The modified error function,  $f^*$ , is

$$f^* = ([D]\{\sigma\} - \{d_0\})^T ([D]\{\sigma\} - \{d_0\}) + ([P]\{\sigma\})^T ([P]\{\sigma\}) \quad (76)$$

where  $[P]$  is a diagonal  $n \times n$  matrix of penalty factors. Each element of  $[P]$  corresponds to one element of  $\{\sigma\}$ . Determination of the elements of  $[P]$  is discussed below.

Setting the derivative of  $f^*$  equal to zero gives the following equation,

$$([A] + [P]^2)\{\sigma\} = \{b\} \quad (77)$$

where  $[A]$  and  $\{b\}$  are the same as in equation (72). Although the additional term in the coefficient matrix of equation (77) changes the solution, it does not change the fact that a unique solution exists and it represents a minimum value of  $f^*$ .

### Decomposition of the Error Function

The vector of approximate displacements given by equation (68) is a full set of displacements for each node in the finite element model. This includes displacements in the x, y, and z coordinate directions and rotations about the x, y, and z coordinate axes. As a practical matter, it may be desired to approximate  $\{d_0\}$  more closely for one degree

of freedom than another. For example, the aerodynamic contour of an aircraft wing must meet very close tolerances in the z direction at every node. In the x, (spanwise), and y, (chordwise), directions there are usually no specific requirements although it may be desirable to minimize the effects of overall growth and fanning to some degree. The rotational degrees of freedom about the x,y, and z axes are not usually specified.

To allow for the possibility of treating each degree of freedom differently,  $\{d_0\}$  and  $[D]$  are decomposed into six parts, each corresponding to one degree of freedom. Each part is scaled by an appropriate factor thereby scaling the corresponding degree of approximation. The modified desired displacement vector and displacement matrix are

$$\{d_0^*\} = k_x\{d_x\} + k_y\{d_y\} + k_z\{d_z\} + k_{rx}\{d_{rx}\} + k_{ry}\{d_{ry}\} + k_{rz}\{d_{rz}\} \quad (78)$$

$$[D^*] = k_x[D_x] + k_y[D_y] + k_z[D_z] + k_{rx}[D_{rx}] + k_{ry}[D_{ry}] + k_{rz}[D_{rz}]. \quad (79)$$

Therefore, by equation (68),

$$\begin{aligned} \{d^*\} = & k_x[D_x]\{\sigma\} + k_y[D_y]\{\sigma\} + k_z[D_z]\{\sigma\} + \\ & k_{rx}[D_{rx}]\{\sigma\} + k_{ry}[D_{ry}]\{\sigma\} + k_{rz}[D_{rz}]\{\sigma\}. \end{aligned} \quad (80)$$

Substituting these into equation (76) and noting that all of the products of displacement matrices  $[D_i]^T [D_j]$  are zero if i is not equal to j, the expression for  $f^*$  becomes

$$\begin{aligned} f^* = & k_x^2(\{d_x\}-[D_x]\{\sigma\})^T (\{d_x\}-[D_x]\{\sigma\}) + \\ & k_y^2(\{d_y\}-[D_y]\{\sigma\})^T (\{d_y\}-[D_y]\{\sigma\}) + \\ & k_z^2(\{d_z\}-[D_z]\{\sigma\})^T (\{d_z\}-[D_z]\{\sigma\}) + \\ & k_{rx}^2(\{d_{rx}\}-[D_{rx}]\{\sigma\})^T (\{d_{rx}\}-[D_{rx}]\{\sigma\}) + \\ & k_{ry}^2(\{d_{ry}\}-[D_{ry}]\{\sigma\})^T (\{d_{ry}\}-[D_{ry}]\{\sigma\}) + \\ & k_{rz}^2(\{d_{rz}\}-[D_{rz}]\{\sigma\})^T (\{d_{rz}\}-[D_{rz}]\{\sigma\}) + \\ & k_p^2([P]\{\sigma\})^T ([P]\{\sigma\}) \end{aligned} \quad (81)$$

where  $k_p$  is a scale factor that may be applied to the matrix of penalty factors,  $[P]$ .

Differentiating  $f^*$  with respect to the stress intensities and setting the result equal to zero gives the following expression for  $\{\sigma\}$ .

$$[A]\{\sigma\} = \{b\} \quad (82)$$

where now

$$\begin{aligned} [A] = & k_x^2 [D_x]^T [D_x] + k_y^2 [D_y]^T [D_y] + k_z^2 [D_z]^T [D_z] + \\ & k_{rx}^2 [D_{rx}]^T [D_{rx}] + k_{ry}^2 [D_{ry}]^T [D_{ry}] + k_{rz}^2 [D_{rz}]^T [D_{rz}] + \\ & k_p^2 [P]^T [P] \end{aligned}$$

and

$$\begin{aligned} \{b\} = & k_x^2 [D_x]^T \{d_x\} + k_y^2 [D_y]^T \{d_y\} + k_z^2 [D_z]^T \{d_z\} + \\ & k_{rx}^2 [D_{rx}]^T \{d_{rx}\} + k_{ry}^2 [D_{ry}]^T \{d_{ry}\} + k_{rz}^2 [D_{rz}]^T \{d_{rz}\}. \end{aligned}$$

To ensure the existence of a unique solution to equation (82), the matrix of penalty factors,  $[P]$ , is required to be positive definite and  $k_p$  is required to be nonzero. The solution corresponds to a minimum value of the modified error function,  $f^*$ , which represents the sum of a scaled error term for each degree of freedom and a scaled stress intensity magnitude term. This solution therefore reflects a compromise between the degree of accuracy desired for each displacement degree of freedom and the magnitudes of the stress intensities.

The relative accuracy of approximation of each degree of freedom can be controlled with the six parameters,  $k_x$ ,  $k_y$ ,  $k_z$ ,  $k_{rx}$ ,  $k_{ry}$ , and  $k_{rz}$ . The magnitudes of the stress intensities can be controlled with the parameter  $k_p$  and the matrix of penalty factors,  $[P]$ . A large value of the scale factor for one degree of freedom relative to the others will result in increased accuracy for that degree of freedom relative to the others. If the scale factor for one degree of freedom is specified as zero, that degree of freedom is effectively removed from consideration. The displacements corresponding to that degree of freedom

are still included in the finite element model but are simply allowed to assume values corresponding to a minimum value of the strain energy in the plate. Likewise, a large value of  $k_p$  or a large value of one of the components of  $[P]$  will tend to reduce the accuracy of the contour and minimize the corresponding stress intensity magnitude.

As mentioned above, the rotational displacements are not usually specified and the  $z$  displacements are always specified. The parameters  $k_{rx}$ ,  $k_{ry}$ , and  $k_{rz}$  may then be taken to be zero and the parameter  $k_z$  is set equal to one. In addition, it is assumed that if desired displacements in the  $x$  and  $y$  directions are to be specified, they will be specified as zero to minimize the effects of flanging and overall growth. The vectors  $\{d_x\}$  and  $\{d_y\}$  are therefore taken to be zero.

Equation (81) becomes

$$f^* = k_x^2([D_x]\{\sigma\})^T ([D_x]\{\sigma\}) + k_y^2([D_y]\{\sigma\})^T ([D_y]\{\sigma\}) + (\{d_z\}-[D_z]\{\sigma\})^T (\{d_z\}-[D_z]\{\sigma\}) + k_p^2([P]\{\sigma\})^T ([P]\{\sigma\}). \quad (83)$$

Equation (82) becomes

$$[A]\{\sigma\} = \{b\} \quad (84)$$

where

$$[A] = k_x^2[D_x]^T[D_x] + k_y^2[D_y]^T[D_y] + [D_z]^T[D_z] + k_p^2[P]^T[P]$$

$$\{b\} = [D_z]^T\{d_z\}.$$

The peening intensity pattern therefore depends on the desired contour through the matrices,  $[D]$ , and  $\{d_0\}$ , and on the specified parameters,  $k_x$ ,  $k_y$ , and  $k_p$ . The matrix of penalty factors must still be calculated.

### Calculation of [P]

Each component of [P] is a penalty factor that corresponds to one component of  $\{\sigma\}$ . The function of the  $P_i$  are to include in the value of  $f^*$  the term,  $(k_p \sigma_i P_i)^2$ . When the minimum of  $f^*$  is calculated,  $\sigma_i$  is minimized to some degree as well. A stress intensity will need to have a larger penalty factor applied if its magnitude exceeds the capabilities of the peening machines. The  $P_i$  are therefore functions of the  $\sigma_i$  making equation (84) nonlinear. The functional form of the  $P_i$  is not known. It is known, however, that if the in-plane stress intensities are negative or if the upper bound on any of the stress intensities is exceeded then the corresponding  $P_i$  are too small and must be increased. An iterative solution is therefore required.

For the first iteration the  $P_i$  are set to very small numbers chosen so that  $f^*$  is dominated by the contour error terms. Equation (84) is then solved for a set of stress intensities. The in-plane stress intensities are checked for negative values and the corresponding penalty factors are incremented by a small amount if necessary. The stress intensities are then substituted into equations (65) and (66) to get the radius of curvature and required growth for each element. Equations (50) and (51) are then used to get the Almen intensities. The Almen intensities are checked against upper bounds and the corresponding penalty factor is incremented if necessary. The stress intensities are then recalculated with the updated penalty factors and the process is repeated. The iterative process is said to have converged when the norm of the vector of stress intensities has stabilized. Experience indicates that the stress intensity norm can fluctuate somewhat. The norm is therefore required to remain within tolerance for several iterations. The procedure is summarized in Figure 24.

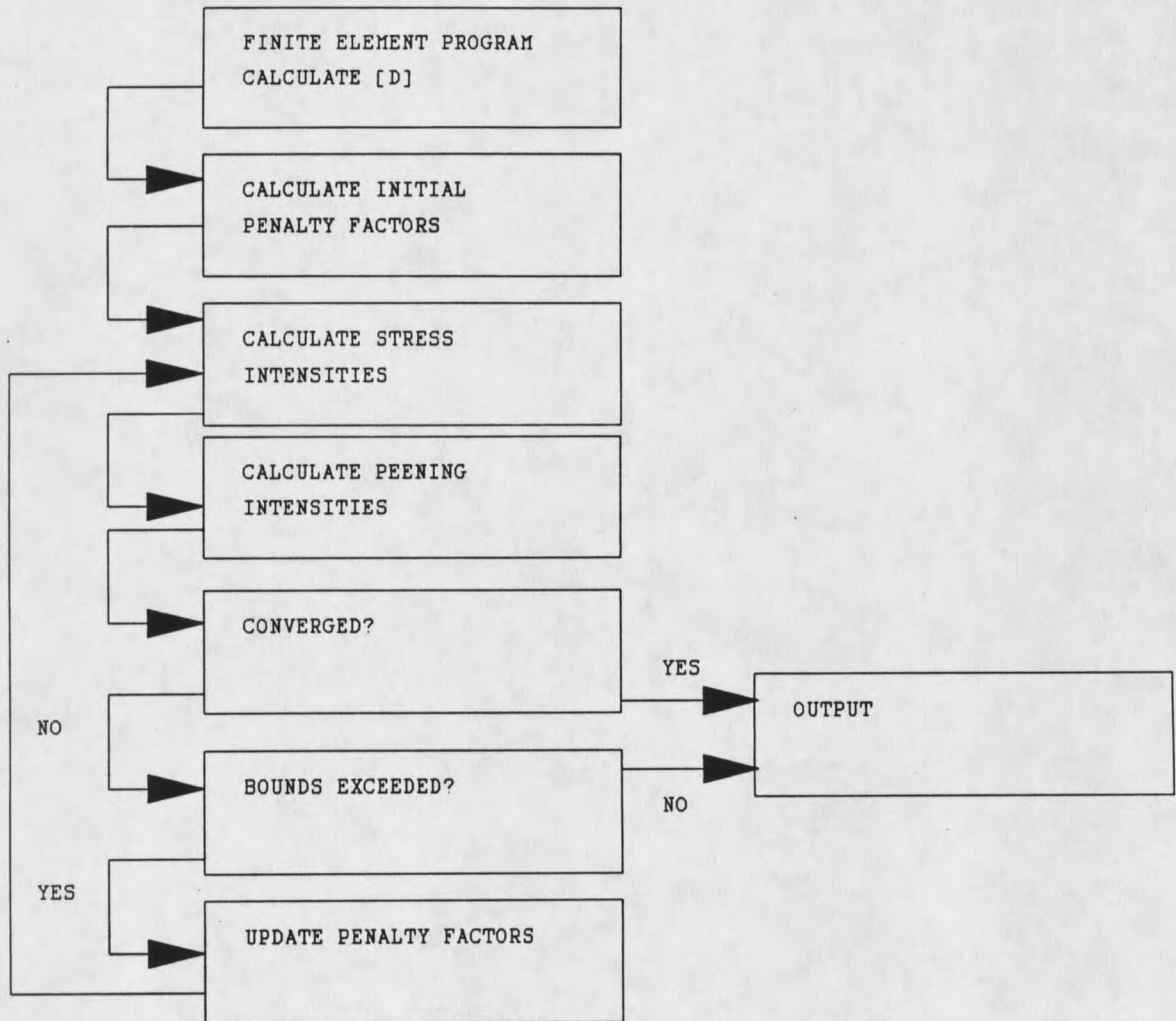


Figure 24. Iterative Procedure for Calculating Peening Intensities.

## CHAPTER V

## RESULTS

In this chapter three example problems are presented and discussed. The example problems have been chosen so that the effect of various contour definitions on the peening pattern can be observed. The first two examples are relatively simple shapes. Example 3 is more complex and is discussed in somewhat more detail. Effects of variation of the penalty scale factor are discussed. The developed system is then applied to a wing skin that is currently in production at The Boeing Company.

Example Problems

In the discussion that follows, all distances, displacements, and contour error values are assumed to have units of inches.

All three examples simulate peening the same flat rectangular plate to achieve different desired contours. The problems, therefore, all use the same finite element model with one exception. Since the stiffness of the plate is calculated in the final configuration, each example plate will have different nodal z coordinates according to the desired contour definition. The finite element portion of the analysis, calculation of the elements of  $[D]$ , must therefore be done separately for each problem. This is true even though the plates are identical in their undeformed configuration.

The example mesh is shown in Figure 25. The plate dimensions are 400 x 40 x 0.2. The model is comprised of 125 4-node quadrilateral thin plate/shell elements and 156 equally spaced nodes. Each element has dimension 16 x 8 x 0.2. Each element also has the same material properties. Poisson's ratio for aluminum,  $\nu = 0.3$ , is used in all three examples.

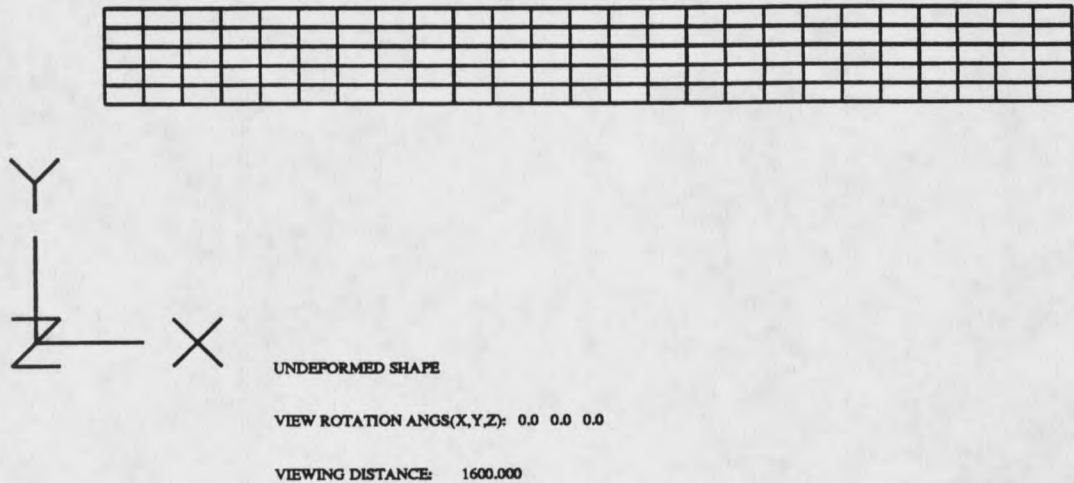


Figure 25. Finite Element Mesh.

Figure 25 also shows the orientation of the global coordinate axes. The origin of the coordinate system is at the lower left hand corner of the plate.

Solution of the peening problem requires that the model be given a set of statically determinate supports. The upper left, lower left, and lower right corner nodes,  $(x,y) = (0,40)$ ,  $(0,0)$ , and  $(400,0)$ , are constrained in the  $z$  direction. These constraints prevent translation in the  $z$  direction and rotation about the  $x$  and  $y$  axes. The lower left and lower right corner nodes,  $(x,y) = (0,0)$  and  $(400,0)$ , are constrained in the  $y$  direction. This

prevents translation in the y direction and rotation about the z axis. Finally, the lower left corner node,  $(x,y) = (0,0)$ , is constrained in the x direction preventing translation in the x direction.

Input to the minimization portion of the analysis consists of a tolerance, values of the scale factors  $k_x$ ,  $k_y$ , and  $k_p$ , and the previously calculated elements of [D]. Since only the z value is specified for the example contours,  $k_x$  and  $k_y$  are set to zero. This allows for maximum accuracy in the contour to be achieved. Fanning and overall growth are not restricted. Values for the tolerance and the penalty scale factor are generally chosen by trial and error for each contour to give the best results. In the following examples, however, the same value is used for each so that only the desired contour is varied. The tolerance is set to 0.0005 and the penalty scale factor,  $k_p$ , is set to 0.2 for all three examples.

#### Example 1 - Twisted Contour

In this example, a twisted contour similar to that of Figure 21 is examined. A constant multiplier is used to limit the desired contour to the realm of small deflections. This example was chosen to contrast the results of the finite element based method with those of the geometric method currently in use at The Boeing Company. The geometric method predicts zero required growth and zero required curvature for the entire plate.

The desired contour is given by the function

$$f(x,y) = 0.00075xy. \quad (85)$$

Note that this function satisfies the boundary conditions required by the three constraints in the z direction. The maximum deflection of 12 occurs at the upper right corner node,  $(x,y) = (400,40)$ . The desired contour is shown in Figure 26.

































































